

Alternating Shrinking Higher-order Interactions for Sparse Neural Population Activity

Ulises Rodríguez-Domínguez ^a, Hideaki Shimazaki ^{a,b},

^a*Graduate School of Informatics, Kyoto University, Japan*

^b*Center for Human Nature, Artificial Intelligence, and Neuroscience (CHAIN), Hokkaido University, Japan*



Abstract

Neurons process sensory stimuli efficiently, showing sparse yet highly variable ensemble spiking activity involving structured higher-order interactions. The occurrence rate of spiking neurons in the population within short time windows also exhibits sparse and widespread distributions. However, how the spiking activities of numerous interacting neurons result in the sparse and widespread population activity remains unknown. Here, we provide sufficient conditions for the joint activity of homogeneous (0,1) binary neurons, resulting in sparse and widespread population rate distributions in infinitely large networks. We then propose a subclass of exponential family distributions in which the sign and magnitude of neurons' higher-order interactions alternate and shrink as the order increases. The models induce parameter-dependent sparsity in the population firing rate distributions on a bounded support. The analysis of recurrent networks that recapitulate the distributions reveals that neurons possess threshold-like nonlinear activation functions to promote sparse activity. The theory establishes sparse distributions for binary patterns, which serve as a building block for developing energy-efficient spike-based learning machines.

Keywords: Sparse distribution, widespread distribution, binary patterns, higher-order interactions, exponential family distribution, neural population activity, nonlinear activation function

1. Introduction

The fundamental constraint placed on neural systems operating in natural environments is efficiency. Neurons therefore exhibit sparsity in various aspects of their activity patterns [1, 2] such as in the distribution of individual neuron responses to multiple stimuli (lifetime sparseness) [3] and the response distribution of a population of neurons (population sparseness) [3, 4, 5]. These sparse

Email addresses: `rodriguezdominguez.ulises.2a@kyoto-u.ac.jp` (Ulises Rodríguez-Domínguez ) , `h.shimazaki@i.kyoto-u.ac.jp` (Hideaki Shimazaki )

distributions require non-trivial higher-order statistical structure. For continuous distributions, sparsity is characterized by the higher-order moments such as kurtosis, which measures the tailedness of the distributions. Many parametric sparse distributions for continuous values have been proposed, often within the context of the Bayesian prior for sparse coding [6]. However, sparse distributions for spiking activities of neurons have not been established. Further, how the sparse profiles in the population distributions arise from the spiking activities of interacting neurons remains elusive.

One approach to understanding cooperative spiking activities of neurons involves analyzing near-simultaneous activities by binarizing the spiking activity within short time windows. When expressed by the exponential family distributions with interactions of multiple orders, this analysis can reveal interactions among subsets of neurons in the population. Interactions among more than two neurons are often termed higher-order interactions (HOIs). The model that lacks HOIs is obtained by constructing a distribution that maximizes entropy while constraining activity rates of individual neurons and joint activity rates of neuron pairs. This model, in which all HOIs are fixed at zero, is called a pairwise maximum entropy (MaxEnt) model (a.k.a, the spin-glass or Ising model in statistical physics and the Boltzmann machine in machine learning). The pairwise MaxEnt model highlights the role of HOIs. The joint activity of more than two neurons produced by this model appears as chance coincidences expected from the activity rates of individual neurons and neuron pairs. Consequently, if nonzero HOIs exist, they indicate deviations in the joint activities of more than two neurons from these chance coincidences.

There is considerable evidence suggesting that HOIs are necessary for characterizing the activity of neural populations. Early in vitro studies reported that the pairwise MaxEnt model accounted for approximately 90% of activity patterns of small populations [7, 8], implying that HOIs made only marginal contributions. However, HOIs may become more prominent as the population size increases [9, 10, 11, 12]. Significant HOIs were later found ubiquitously in both in vitro and in vivo neurons [13, 14, 11, 15, 16]. Analyzing HOIs enables researchers to uncover the underlying circuitry [17] and provides insights into their stimulus coding [18, 19, 14, 15, 20].

One of the most striking features involving HOIs is the widespread distribution of neural activity. A widespread or non-concentrated distribution is a distribution whose probability mass is not concentrated at a single point but spread across its support. Spike-count histograms for the number of simultaneously active neurons often exhibit widespread distributions, with notably longer tails for probabilities in highly synchronous states compared to independent or pairwise MaxEnt models [11, 15]. These observations underscore the importance of HOIs in realizing the widespread population spike-count histograms. Furthermore, the high variabilities of the probabilities (i.e., the high variance of log probabilities) lead to increased heat capacity, which indicates that the HOIs facilitate neural systems transitioning to highly fluctuating regimes and may bring the systems to a critical state [21].

At the same time, spike-count distributions of neurons in various brain re-

gions exhibit sparsity. Evidence for this can be found in the spike-count histogram of individual neurons, such as retinal ganglion cells [22], V1 neurons [23], and primary auditory cortex neurons [24]. Population-level histograms of neural activity also display sparse profiles. Neurons are only sparsely active over time, with the duration of a state in which all neurons are silent being significantly longer than the prediction made by the pairwise MaxEnt model in both in vitro [10, 11, 16] and in vivo [15, 14, 25] studies. The study in [16] showed that the simultaneous silence is a dominant factor representing the HOIs, resulting in the alternating structure with positive pairwise, negative triple-wise, and positive quadruple-wise interactions when the activity is represented by $(0, 1)$. The study in [17] revealed that the leaky integrate-and-fire neurons receiving local excitatory common inputs can produce the sparse population activity with the positive pairwise and negative triple-wise interactions observed in visual neurons while neurons receiving common inhibition can not, suggesting that the threshold nonlinearity of neurons plays a key role in yielding the observed sparse population activity.

While it is evident that HOIs are involved in sparse, widespread distributions, yet sufficient conditions and parametric models for such distributions remain unestablished. In this study, we establish sufficient conditions resulting in sparse and widespread distributions for spiking activities of a homogeneous neural population. Based on the theory, we introduce new parametric models belonging to the exponential family distribution with structured alternating and shrinking higher-order interactions that yield sparse and widespread population rate distributions in the limit of a large number of neurons. The necessity of non-zero higher-order interactions in constructing the widespread distributions was pointed out by Amari et al. [26]. Unlike the previous study, we show that the base measure function in the exponential family distribution is vital for canceling the entropy term of the combinatorial patterns that may otherwise dominate in the population spike-count histograms.

Interpretation from the dynamics of a recurrent neural network that behaves as a sampler of the sparse distributions described above reveals that the neurons possess sublinear, threshold-like, nonlinear activation functions. Such nonlinearity promotes sparse population activity and may be realized as a computation performed at the dendrites on top of the spike-generation nonlinearity at the axon hillock of soma. From a machine learning point of view, the proposed models are variants of the Boltzmann machines that extend their capacity by capturing the higher-order dependency on inputs (e.g., restricted Boltzmann machines [27]). Recently, specific nonlinearities inducing the higher-order interactions are introduced in the context of the modern Hopfield networks [28, 29]. They have higher memory capacity than the classical Ising networks, and their nonlinearity has relevance to the Transformers [30] and diffusion models [31]. The present theory that establishes sparse distributions for binary patterns will serve as a building block for developing prior distributions for energy-efficient spike-based sparse coding in machine learning and further provide implications on the sparse nonlinearity to enhance modern learning machines.

The paper is organized as follows. In Section 2, we describe a probability

mass function (PMF) of $(0, 1)$ binary patterns using the exponential family distribution, assuming homogeneity over the neurons, and construct a population-count histogram, a distribution of the total activity in the population. We provide sufficient conditions that make a distribution widespread with its peak at a population spike count of zero in the limit of a large number of neurons. In Section 3, we show how a common scenario for homogeneous MaxEnt models leads to the widespread property being hindered due to entropy domination in the PMF for a large number of neurons. Then, in Section 4, we introduce our alternating shrinking higher-order interaction models, whose corresponding probability density functions (PDFs) become widespread and remain sparse in the limit of a large number of neurons. In this section, we also interpret the proposed models from the perspective of recurrent neural networks having an extended nonlinearity and compare the models against their first and second-order interaction counterparts when fitting to the spiking activity of in vitro neurons. We conclude with a discussion in Section 5.

2. Homogeneous sparse population of neurons

The activity of N neurons is represented by a set of binary random variables, using a column vector, $\mathbf{X} = [X_1, X_2, \dots, X_N]^T$ where $X_i \in \{0, 1\}$ and for which we assume stationarity. The i th neuron activity X_i is 1 if the neuron is active and 0 otherwise. The probabilities of generating binary activity patterns, specified by $\mathbf{x} = [x_1, x_2, \dots, x_N]^T$, where $x_i \in \{0, 1\}$ are given as $\mathcal{P}(\mathbf{X} = \mathbf{x})$. This PMF can be written in the form of an exponential family distribution:

$$\mathcal{P}(\mathbf{X} = \mathbf{x}) = \frac{h(\mathbf{x})}{Z} \exp \left[\sum_{i=1}^N \theta_i x_i + \sum_{i_1 < i_2} \theta_{i_1 i_2} x_{i_1} x_{i_2} + \sum_{i_1 < i_2 < i_3} \theta_{i_1 i_2 i_3} x_{i_1} x_{i_2} x_{i_3} + \dots + \theta_{12\dots N} x_{i_1} \dots x_{i_N} \right], \quad (1)$$

where Z is a normalization term, and the parameters $\{\theta_i\}_{i=1}^N$, $\{\theta_{i_1 i_2}\}_{i_1 < i_2}$, \dots , $\theta_{1\dots N}$ are called natural parameters. They characterize interactions among subset neurons indicated by the subscript indices [32, 33]. The exponential family distribution allows the base measure function $h(\mathbf{x})$ to be a general nonnegative function of the vector pattern \mathbf{x} . Here, we will assume that $h(\mathbf{x})$ is a function of the total activity, $\sum_{i=1}^N x_i$. Although Eq. 1 can realize arbitrary probabilities for all possible patterns even if $h(\mathbf{x}) = 1$, as we will show, the introduction of an appropriate base measure function simplifies the conditions for the sparse widespread distributions and for modeling the neural interactions. For simplicity, we use $\mathcal{P}(\mathbf{x})$ to represent $\mathcal{P}(\mathbf{X} = \mathbf{x})$.

We study the activity of a population of homogeneous neurons. Homogeneity is an important assumption for which specific preference over some neural

activity patterns is ignored. Nonetheless, homogeneity allows us to change the analysis focus from a local to a global view of the sparse neural population activity in a region, facilitating the identification of theoretical properties. The binary activity of the homogeneous population is described by using single parameters θ_k ($k = 1, 2, \dots, N$) for all the combinatorial k -th order interactions in Eq. (1)

$$\mathcal{P}(\mathbf{x}|\boldsymbol{\theta}_N) = \frac{h\left(\sum_{i=1}^N x_i\right)}{Z} \exp\left[\theta_1 \sum_{i=1}^N x_i + \theta_2 \sum_{i_1 < i_2} x_{i_1} x_{i_2} + \dots + \theta_N x_{i_1} x_{i_2} \dots x_{i_N}\right], \quad (2)$$

where $\boldsymbol{\theta}_N = (\theta_1, \theta_2, \dots, \theta_N)$. This model extends the theoretical work by Amari et al. [26], where $h\left(\sum_{i=1}^N x_i\right) = 1$. The population activity of the homogeneous neurons is characterized by the distribution of the number of active neurons in the population. For homogeneous neurons, any individual binary pattern where n neurons are active has the same probability. Therefore, the probability of having n number of active neurons in the population is given by

$$\begin{aligned} \mathcal{P}\left(\sum_{i=1}^N X_i = n \mid \boldsymbol{\theta}_N\right) &= \binom{N}{n} \mathcal{P}(x_1 = 1, \dots, x_n = 1, x_{n+1} = 0, \dots, x_N = 0 \mid \boldsymbol{\theta}_N) \\ &= \binom{N}{n} \frac{h(n)}{Z} \exp\left[\binom{n}{1} \theta_1 + \binom{n}{2} \theta_2 + \dots + \binom{n}{n} \theta_n\right] \\ &= \binom{N}{n} \frac{h(n)}{Z} \exp\left[\sum_{k=1}^n \binom{n}{k} \theta_k\right]. \end{aligned} \quad (3)$$

Let the fraction of active neurons (or population rate) be $R_N = \frac{1}{N} \sum_{i=1}^N X_i$. Using Eq. (3), the PMF of the random variable R_N , $\mathcal{P}(R_N = r_N \mid \boldsymbol{\theta}_N)$, where $r_N \in S_r$ with $S_r \equiv \{0, \frac{1}{N}, \frac{2}{N}, \dots, 1\}$, is

$$\begin{aligned} \mathcal{P}(R_N = r_N \mid \boldsymbol{\theta}_N) &= \mathcal{P}\left(\sum_i X_i = Nr_N \mid \boldsymbol{\theta}_N\right) \\ &= \binom{N}{Nr_N} \frac{h(Nr_N)}{Z} \exp\left[\sum_{k=1}^{Nr_N} \binom{Nr_N}{k} \theta_k\right]. \end{aligned} \quad (4)$$

We call this a PMF of the discrete population rate, and we rewrite it as

$$\mathcal{P}(R_N = r_N \mid \boldsymbol{\theta}_N) = \frac{1}{Z} \exp[NG_N(r_N; \boldsymbol{\theta}_N)], \quad (5)$$

where

$$G_N(r_N; \boldsymbol{\theta}_N) = \frac{1}{N} \log \binom{N}{Nr_N} + \frac{1}{N} \log h(Nr_N) + \frac{1}{N} Q_N(r_N; \boldsymbol{\theta}_N), \quad (6)$$

and with the polynomial term defined as

$$Q_N(r_N; \boldsymbol{\theta}_N) = \sum_{k=1}^{Nr_N} \binom{Nr_N}{k} \theta_k. \quad (7)$$

We note that the new underlying base measure function for such population rate distribution (Eq. (4)) consists of the binomial term multiplied by the $h(\cdot)$ function, i.e., $\binom{N}{Nr_N} h(Nr_N)$. As we stated before, such base measure function could alternatively be represented in a different way inside the (possibly non-polynomial) function $Q_N(\cdot)$ as a function of the active neurons given the canonical parameters. Nonetheless, the representation we chose facilitates analysis in the limit of a large population of neurons as we will see. In the following, we use $\mathcal{P}(r_N|\boldsymbol{\theta}_N)$ to represent the PMF above.

We are interested in the behavior of the PMF (Eq. (5)) in the limit of a large number of neurons ($N \rightarrow \infty$): Namely, the probability density function (PDF) given through the relation $p(r|\boldsymbol{\lambda}) dr = \lim_{N \rightarrow \infty} \mathcal{P}(r_N|\boldsymbol{\theta}_N)$, where r is the continuous population rate defined in the support $[0, 1]$ and $\boldsymbol{\lambda}$ is the set of parameters for the PDF. We wish to know the conditions under which this PDF is sufficiently concentrated, near its peak of 0. Such a PDF would be relevant to model experimentally observed sparse population activity across different cortical populations, where arbitrarily low firing rates were exhibited by most neurons [34]. Following Amari et al.'s framework to construct widespread distributions [26], we provide a new theorem below giving sufficient conditions for sparse and widespread distributions.

Theorem 1. *Let $G_N(r_N; \boldsymbol{\theta}_N)$ be a non-positive strictly decreasing function with finite values for $r_N \in S_r$. If $NG_N(r_N; \boldsymbol{\theta}_N)$ has the following order of magnitude in terms of N ,*

$$\mathcal{O}(NG_N(r_N; \boldsymbol{\theta}_N)) = \mathcal{O}(1), \quad (8)$$

then the corresponding probability density function given through $p(r|\boldsymbol{\lambda}) dr = \lim_{N \rightarrow \infty} \mathcal{P}(r_N|\boldsymbol{\theta}_N)$ is widespread in $(0, 1]$ with a single non-concentrated maximum at 0.

For proof, the reader can refer to Appendix A.1.

Specifically, if we have the following form for the function $h(\mathbf{x})$:

$$h\left(\sum_{i=1}^N x_i\right) = 1 / \binom{N}{\sum_{i=1}^N x_i} \quad (9)$$

then the first two terms in Eq. (6) cancel out, resulting in

$$G_N(r_N; \boldsymbol{\theta}_N) = \frac{1}{N} Q_N(r_N; \boldsymbol{\theta}_N). \quad (10)$$

Thus, we obtain the following corollary:

Corollary 1. *Let $h(\mathbf{x})$ be given by Eq. (9). If the polynomial term $Q_N(r_N; \boldsymbol{\theta}_N)$ satisfies*

$$\mathcal{O}(Q_N(r_N; \boldsymbol{\theta}_N)) = \mathcal{O}(1), \quad (11)$$

and if $q(r; \boldsymbol{\lambda}) = \lim_{N \rightarrow \infty} Q_N(r_N; \boldsymbol{\theta}_N)$ is a non-positive strictly decreasing function, then the probability density function $p(r|\boldsymbol{\lambda})$ is widespread in $(0, 1]$ with a single non-concentrated maximum at 0.

We introduce the two simplest homogeneous sparse models in the following subsection (Subsection 2.1). Then, in Section 3, we present a common scenario to which Theorem 1 does not apply, resulting in a concentrated distribution. In Section 4, we present our proposed model whose population rate PMF is a particular case of Eq. (5). The distribution satisfies the conditions in Theorem 1 and converges to a widespread continuous distribution with parameter-dependent sparsity.

2.1. First and second-order homogeneous sparse models

Here, we introduce the simplest homogeneous model able to produce sparse population activity, i.e., a homogeneous population of binary neurons with only the first-order parameters ($\theta_2 = \theta_3 = \dots = \theta_N = 0$). Using $\theta_1 = -f/N$, the PMF of the binary population is given as

$$\mathcal{P}(\mathbf{x}|f) = \frac{h\left(\sum_{i=1}^N x_i\right)}{Z} \exp\left[-f \frac{\sum_{i=1}^N x_i}{N}\right], \quad (12)$$

where we assume that $f > 0$ and the function $h(\cdot)$ is given by Eq. (9). With this $h(\cdot)$ function that cancels out with the binomial term in Eq. (6), the corresponding population rate PMF (Eq. (5)) is given as

$$\mathcal{P}(r_N|\theta_1) = \frac{1}{Z} e^{-fr_N}. \quad (13)$$

The corresponding continuous PDF is obtained through

$$p(r|f) dr = \lim_{N \rightarrow \infty} \mathcal{P}(r_N|\theta_1) = \frac{1}{Z} e^{-fr} dr, \quad (14)$$

where the normalization constant is obtained as

$$Z = \int_0^1 e^{-fr} dr = \frac{1 - e^{-f}}{f}. \quad (15)$$

Since $\mathcal{O}(-fr_N) = \mathcal{O}(1)$ and $q(r; f) = -fr$ is a strictly decreasing function, the PDF in Eq. (14) is widespread in $(0, 1]$ with a single non-concentrated maximum at 0 (Corollary 1). The sparsity in such PDF is controlled by the f parameter. See Appendix A.2 for the distribution's mean and variance.

This density corresponds to the PDF of an exponential distribution with parameter $f > 0$ but with a compact support in $[0, 1]$, instead of the support in

$[0, \infty)$. This first-order model serves as a baseline for investigating the effect of the pairwise and higher-order interactions in shaping the sparse distribution.

As the second simplest homogeneous model, we obtain the canonical parameters $\theta_1 = \frac{f_1}{N} + \frac{f_2}{N^2}$ and $\theta_2 = 2\frac{f_2}{N^2}$, which leads to a polynomial $Q_N(r_N; \boldsymbol{\theta}_N) = f_1 r_N + f_2 r_N^2$ independent of N . Thus, using again Eq. (9) for $h(\cdot)$ we obtain a continuous PDF as

$$p(r|f_1, f_2) dr = \lim_{N \rightarrow \infty} \mathcal{P}(r_N|\theta_1, \theta_2) = \frac{1}{Z} \exp[f_1 r + f_2 r^2] dr, \quad (16)$$

where the normalization constant is obtained as

$$Z = \int_0^1 e^{f_1 r + f_2 r^2} dr = \begin{cases} \frac{\sqrt{\pi}}{2\sqrt{f_2}} \exp\left[-\left(\frac{f_1}{2\sqrt{f_2}}\right)^2\right] \operatorname{erfi}\left(\frac{f_1}{2\sqrt{f_2}} + \sqrt{f_2}r\right) \Big|_0^1 & \text{if } f_2 > 0 \\ \frac{\sqrt{\pi}}{2\sqrt{|f_2|}} \exp\left[\left(\frac{f_1}{2\sqrt{|f_2|}}\right)^2\right] \operatorname{erf}\left(-\frac{f_1}{2\sqrt{|f_2|}} + \sqrt{|f_2|}r\right) \Big|_0^1 & \text{if } f_2 < 0 \end{cases}, \quad (17)$$

where the imaginary error function $\operatorname{erfi}(\cdot)$ is defined as

$$\operatorname{erfi}(x) = \sum_{k=0}^{\infty} \frac{x^{2k+1}}{(2k+1)k!}, \quad (18)$$

and the error function $\operatorname{erf}(\cdot)$ as

$$\operatorname{erf}(x) = \sum_{k=0}^{\infty} \frac{(-1)^k x^{2k+1}}{(2k+1)k!}. \quad (19)$$

3. Entropy-dominated homogeneous population

This section shows that the condition $h(\mathbf{x}) = 1$, commonly used in the standard homogeneous pairwise MaxEnt model, fails the entropy cancellation, resulting in a concentrated distribution.

We now analyze the behavior of the homogeneous PMF (Eq. (5)) with $h(Nr_N) = 1$ as the number of neurons N grows to infinity while keeping the order of the polynomial part $Q_N(r_N; \boldsymbol{\theta}_N)$ constant in N , i.e.,

$$\mathcal{O}(Q_N(r_N; \boldsymbol{\theta}_N)) = \mathcal{O}(1). \quad (20)$$

Coupled with the Stirling formula for factorials using the order notation, i.e.,

$$N! = \sqrt{2\pi N} \left(\frac{N}{e}\right)^N \left(1 + \mathcal{O}\left(\frac{1}{N}\right)\right), \quad (21)$$

the function $G_N(\cdot; \boldsymbol{\theta}_N)$ from the PMF (Eq. (5)) for $r_N \neq 0$ and $r_N \neq 1$ becomes (see Appendix B for the details)

$$G_N(r_N; \boldsymbol{\theta}_N) = -\frac{1}{N} \log \sqrt{2\pi N r_N (1 - r_N)} + H(r_N) + \frac{1}{N} Q_N(r_N; \boldsymbol{\theta}_N) + \frac{1}{N} \mathcal{O}\left(\frac{1}{N}\right), \quad (22)$$

where $H(r_N)$ is the entropy term, defined as

$$H(r_N) = -r_N \log(r_N) - (1 - r_N) \log(1 - r_N). \quad (23)$$

Because the entropy order $\mathcal{O}(H(r_N)) = \mathcal{O}(1)$ is constant and considering Eq. (20), then the order of the function $NG_N(r_N; \boldsymbol{\theta}_N)$ is

$$\begin{aligned} & \mathcal{O}\left(-\log \sqrt{2\pi N r_N (1 - r_N)} + NH(r_N) + Q_N(r_N; \boldsymbol{\theta}_N) + \mathcal{O}\left(\frac{1}{N}\right)\right) \\ &= \mathcal{O}\left(-\sqrt{N} + N + 1 + \frac{1}{N}\right) \\ &= \mathcal{O}(N). \end{aligned} \quad (24)$$

Eq. (24) is the linear order of N because the entropy term dominates over the other terms for large N .

The dominance of the entropy as $N \rightarrow \infty$ leads to the following delta PDF

$$\begin{aligned} \lim_{N \rightarrow \infty} \mathcal{P}(r_N | \boldsymbol{\theta}_N) &= p(r | r^*) dr \\ &= \delta(r - r^*) dr, \end{aligned} \quad (25)$$

whose peak is concentrated at its maximum r^* in the region dominated by the entropy. The corresponding distribution function is

$$\begin{aligned} \lim_{N \rightarrow \infty} F(r_m | r^*) &= \int_0^{r_m} \delta(r - r^*) dr \\ &= u(r_m - r^*), \end{aligned} \quad (26)$$

where $u(\cdot)$ denotes the heavyside step function. For a proof of Eqs. (25) and (26) see Appendix B.

The result above proves that with $h(\mathbf{x}) = 1$ the distribution concentrates without canceling the entropy, unlike $h(\mathbf{x})$ given by Eq. (3). Different base measure functions in the exponential family for the binary patterns correspond to different base measure functions of the homogeneous population models (discrete or continuous). We summarize these correspondences in Table 1. Note that the base measure function of the homogeneous continuous population rate model approaches the delta function if we use $h(\mathbf{x}) = 1$. In this case, the limiting PDF is written by this base measure function alone (25).

We also note that most existing models, e.g., the K-pairwise maximum entropy model by Tkacik et al. [11, 21] and the dichotomized Gaussian (DG)

$h(\cdot)$ function in $\mathcal{P}(\mathbf{x} \boldsymbol{\theta}_N)$	Base measure function	
	$\mathcal{P}(r_N \boldsymbol{\theta}_N)$	$p(r \boldsymbol{\lambda})$
Eq. (9)	1	1
1	$\sqrt{2\pi r_N(1-r_N)} \exp[NH(r_N)]$	$\delta(r-r^*)$

Table 1: The base measure functions of the population rate models for two choices of the $h(\cdot)$ function.

model [26] that result in the widespread distributions, do not explicitly define a base measure function for the binary patterns. According to our theory, when the discrete homogeneous distributions exhibit the widespread property (in the continuous limit), their corresponding function, $h(Nr_N)$, must contain an equivalent component that cancels with the entropy.

Alternatively, we may introduce a parameter that relatively weights the entropy term and the pattern probabilities and consider that the models with widespread distributions are realized at a precisely tuned parameter. The authors in [35] analyzed the homogeneous DG model by introducing a non-canonical parameter β that scales the pattern distribution as $\mathcal{P}_\beta(\mathbf{x}|\boldsymbol{\theta}_N) = \mathcal{P}(\mathbf{x}|\boldsymbol{\theta}_N)^\beta / Z_\beta$, which sets an imbalance between the entropy term $H(r_N)$ and the one that comes from $h(Nr_N)^\beta$. The widespread distribution is only possible at $\beta = 1$ in the limit of N , and they reported it as a phase transition along the parameter.

4. The model with alternating and shrinking higher-order interactions

Neuronal populations exhibit a significant excess rate of simultaneous silence [14, 10, 11, 16], where all neurons become inactive, compared to the chance level predicted by the pairwise MaxEnt models. When expressed in $(0, 1)$ patterns, the probability of silence of all neurons is captured by the feature given by $\prod_{i=1}^N (1-x_i)$ of the exponential family distribution. The model of the excessive simultaneous silence was proposed by adding this term to the pairwise maximum entropy model, $p(\mathbf{x}|\boldsymbol{\theta}) \propto \exp[\sum_i \theta_i x_i + \sum_{i,j} \theta_{i,j} x_i x_j + \theta_0 \prod_{i=1}^N (1-x_i)]$ [16], where the expansion of the silence feature leads to the HOIs with alternating signs for each order,

$$\theta_0 \prod_{i=1}^N (1-x_i) = \theta_0 - \theta_0 \sum_i x_i + \theta_0 \sum_{i,j} x_i x_j - \theta_0 \sum_{i,j,k} x_i x_j x_k + \theta_0 \sum_{i,j,k,l} x_i x_j x_k x_l - \dots \quad (27)$$

However, the simultaneous silence model is limited in that it captures only a state of total silence, whose measure becomes negligibly small for a large number

of neurons and does not yield a widespread population rate distribution in the limit of a large number of neurons. Instead, we show that the following model with the alternating higher-order interactions whose strength shrinks as the order increases with an appropriate base measure function can result in a sparse widespread population rate distribution.

To construct a sparse model with the widespread property in the large N limit, we consider the following distribution for the activity patterns of the homogeneous population of binary neurons:

$$\mathcal{P}(\mathbf{x}|\boldsymbol{\omega}) = \frac{h\left(\sum_{i=1}^N x_i\right)}{Z} \exp\left[-f \sum_{j=1}^N (-1)^{j+1} C_j \left(\frac{\sum_{i=1}^N x_i}{N}\right)^j\right], \quad (28)$$

where $\boldsymbol{\omega} = \{f, C_1, C_2, \dots, C_N\}$ is the set of parameters and Z is its partition function. We assume that $f > 0$ and C_j are positive ($C_j > 0$) and decreasing with respect to j , $C_j < C_{j-1} \quad \forall j = 2, \dots, N$. Combined with $(-1)^{j+1}$, such coefficients impose an alternating structure whose magnitude shrinks as the order of interaction increases. We will provide specific choices of C_j that make the alternating terms in the exponent converge to a decreasing function with respect to r_N . In this model, we use Eq. (9) for the base measure function $h(\mathbf{x})$. Using such a function is one of the sufficient conditions required for the distribution to become widespread in the limit of a large number of neurons (Theorem 1). Therefore, the population rate PMF becomes (see Eq. (10))

$$\mathcal{P}(r_N|\boldsymbol{\theta}_N) = \frac{1}{Z} \exp[Q_N(r_N; \boldsymbol{\theta}_N)], \quad (29)$$

where $Q_N(r_N; \boldsymbol{\theta}_N)$ is a polynomial given by Eq. (7), which will be calculated as follows.

The canonical form of the homogeneous population activity is given by Eq. (2). From Eq. (28), the canonical parameters (θ_k , with the interaction of the order k) of the alternating and shrinking interaction model are computed as

$$\begin{aligned} \theta_1 &= \sum_{l=1}^N (-1)^l \frac{f C_l}{N^l}, \\ \theta_2 &= \sum_{l=2}^N (-1)^l \frac{f C_l}{N^l} \sum_{\substack{k_1+k_2=l \\ k_1>0, k_2>0}} \binom{l}{k_1, k_2}, \\ \theta_3 &= \sum_{l=3}^N (-1)^l \frac{f C_l}{N^l} \sum_{\substack{k_1+k_2+k_3=l \\ k_1>0, k_2>0, k_3>0}} \binom{l}{k_1, k_2, k_3}, \\ &\vdots \\ \theta_N &= (-1)^N \frac{f C_N}{N^N} N!. \end{aligned} \quad (30)$$

See Appendix C.1 for the detailed derivation. We note that in addition to the alternating shrinking behavior for the coefficients in the PMF from Eq. (28), the canonical parameters for the homogeneous PMF (Eq. (2)) also show the alternating shrinking property. This can be seen from Eq. (30), where for each θ_k , its coefficient with the largest magnitude (or dominant) is at $l = k$ for large N . Then, the dominant term for θ_1 is negative, for θ_2 is positive and with smaller magnitude than that of θ_1 , and so on for θ_3 until θ_N .

The PMF of the discrete population rate (Eq. (29)) will be specified by using these canonical parameters, $\boldsymbol{\theta}_N = (\theta_1, \dots, \theta_N)$, where these parameters appear in the polynomial term, $Q_N(r_N; \boldsymbol{\theta}_N)$ (Eq. (7)). Consequently, Eq. (30) is required to obtain (non-trivially) the following form of the polynomial term, computed as

$$Q_N(r_N; \boldsymbol{\theta}_N) = -f \sum_{j=1}^{Nr_N} (-1)^{j+1} C_j (r_N)^j + \mathcal{O}\left(\frac{1}{N}\right). \quad (31)$$

See Appendix C.2 for the derivation. We use this form of the polynomial (Eq. (31)) to formally show how a widespread sparse PDF emerges, which follows next.

In the limit of $N \rightarrow \infty$, our population rate PMF becomes the continuous density given by (see Appendix C.3)

$$\begin{aligned} \lim_{N \rightarrow \infty} \mathcal{P}(r_N | \boldsymbol{\theta}_N) &= p(r | \boldsymbol{\lambda}) dr \\ &= \frac{1}{Z} \exp \left[-f \sum_{j=1}^{\infty} (-1)^{j+1} C_j r^j \right] dr, \end{aligned} \quad (32)$$

where $\boldsymbol{\lambda} = \left\{ f, \{C_j\}_{j \in \mathbb{N}^+} \right\}$. Depending on the choice of each C_j , we obtain different types of densities. Here we provide two examples where the polynomial term $Q_N(r_N; \boldsymbol{\theta}_N)$ converges to a non-positive decreasing function with respect to r , and therefore the corresponding densities result in widespread distributions with a non-concentrated maximum at 0 (Corollary 1).

Polylogarithmic exponential distribution If we define $C_j = \frac{1}{j^m} \forall j$ then the probability density function in Eq. (32) is

$$p(r | f, m) = \frac{1}{Z} \exp [f \text{Li}_m [-r]], \quad (33)$$

where $\text{Li}_m[\cdot]$ is the polylogarithm function of order $m = 1, 2, 3, \dots$ (See Appendix C.3). We call the density in Eq. (33) the polylogarithmic exponential density, where the function $f \text{Li}_m [-r]$ is non-positive (see Appendix D.1) and strictly decreasing (see Appendix D.2) for $r \in [0, 1]$ with a maximum at $r = 0$. See Fig. 1 for the density functions for different f and m . Note that for $m = 1$, we obtain the natural logarithm, i.e.,

$$\text{Li}_1 [-r] = -\log [1 + r]. \quad (34)$$

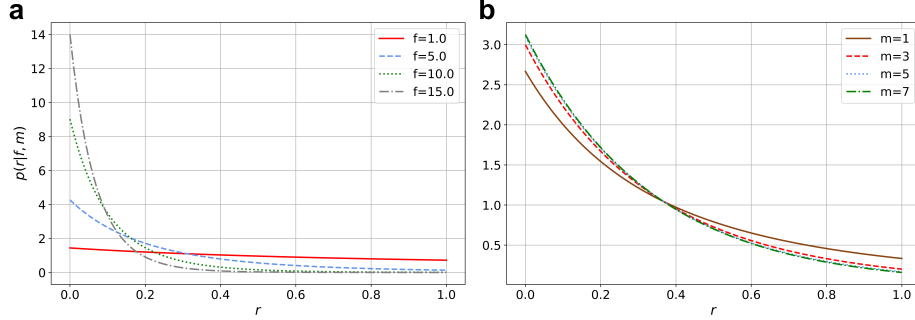


Figure 1: The polylogarithmic exponential PDF. **a** The PDFs for different values of f ($m = 1$). **b** The PDFs for different values of m ($f = 3$).

The distribution function of the polylogarithmic exponential density corresponding to the PDF in Eq. (33) is as follows

$$F(u|f, m) = \frac{1}{Z} \int_0^u \exp(f \text{Li}_m[-r]) dr, \quad (35)$$

where $u \in [0, 1]$. For $m = 1$, we obtain the distribution function

$$F(u|f, m=1) = \frac{1}{Z} \int_0^u \exp(-f \log(1+r)) dr = \begin{cases} \frac{1-(1+u)^{-f+1}}{1-2^{-f+1}} & \text{for } f \neq 1 \\ \frac{\log(1+u)}{\log 2} & \text{for } f = 1. \end{cases} \quad (36)$$

For $m = 2, 3, 4, \dots$, one may employ a numerical integration method to approximate Eq. (35).

The mean of this distribution for $m = 1$ is given by

$$\mu_R = \begin{cases} \frac{1}{Z} \int_0^1 (1+r)^{-f} r dr = \frac{1}{1-2^{-f+1}} \left[\frac{1-2^{-f+2}}{f-2} - 2^{-f+1} \right] & \text{for } f \neq 1 \\ \frac{1}{Z} \int_0^1 (1+r)^{-1} r dr = \frac{1-\log 2}{\log 2} & \text{for } f = 1, \end{cases} \quad (37)$$

and the variance is

$$\sigma_R^2 = \frac{1}{Z} \int_0^1 (1+r)^{-f} r^2 dr - \mu_R^2 = \begin{cases} \frac{1}{1-2^{-f+1}} \left[\frac{2(1-2^{-f+3})}{(f-3)(f-2)} - 2^{-f+1} \left(1 + \frac{2^2}{f-2} \right) \right] - \mu_R^2 & \text{for } f \neq 1 \\ \frac{\log 2 - \frac{1}{2}}{\log 2} - \left[\frac{1-\log 2}{\log 2} \right]^2 & \text{for } f = 1. \end{cases} \quad (38)$$

Shifted-geometric exponential distribution If we instead define $C_j = (\tau)^j$, with $0 < \tau < 1$, $\forall j$ so that $\tau r < 1$, then the probability density function in Eq. (32) is

$$\begin{aligned} p(r|f, \tau) &= \frac{1}{Z} \exp \left[-\frac{f}{1 + \frac{1}{\tau r}} \right] \\ &= \frac{1}{Z} \exp \left[f \left(\frac{1}{1 + \tau r} - 1 \right) \right], \end{aligned} \quad (39)$$

where the last exponential argument corresponds to a shifted-geometric series. See Appendix C.3 for the details. Therefore, we call the density in Eq. (39) the shifted-geometric exponential density. See Fig. 2 for the density functions for different f and τ . In addition, the function $f \left(\frac{1}{1 + \tau r} - 1 \right)$ in Eq. (39) is non-positive (see Appendix D.1) and strictly decreasing (see Appendix D.2) for $r \in [0, 1]$ with a maximum at $r = 0$.

The distribution function corresponding to the shifted-geometric exponential density in Eq. (39) is calculated as

$$\begin{aligned} F(u|f, \tau) &= \frac{1}{Z} \int_0^u \exp \left[f \left(\frac{1}{1 + \tau r} - 1 \right) \right] dr \\ &= \frac{(1 + \tau u) \exp \left[f \left(\frac{1}{1 + \tau u} - 1 \right) \right] - 1 + f e^{-f} \left\{ \text{Ei}(f) - \text{Ei} \left(\frac{f}{1 + \tau u} \right) \right\}}{(1 + \tau) \exp \left[f \left(\frac{1}{1 + \tau} - 1 \right) \right] - 1 + f e^{-f} \left\{ \text{Ei}(f) - \text{Ei} \left(\frac{f}{1 + \tau} \right) \right\}}. \end{aligned} \quad (40)$$

Here, the special exponential integral function $\text{Ei}(x)$ is defined as follows for $x \in \mathbb{R}$ [36]

$$\text{Ei}(x) = \gamma + \log(x) + \sum_{k=1}^{\infty} \frac{x^k}{k k!}, \quad (41)$$

where γ is the Euler-Mascheroni constant ($\gamma \approx 0.5772156649$). See Appendix D.3 for verification of Eq. (40).

The mean value and the variance of this distribution are given by

$$\mu_R = \frac{1}{Z} \int_0^1 \exp \left[f \left(\frac{1}{1 + \tau r} - 1 \right) \right] r dr, \quad (42)$$

and

$$\sigma_R^2 = \frac{1}{Z} \int_0^1 \exp \left[f \left(\frac{1}{1 + \tau r} - 1 \right) \right] r^2 dr - \mu_R^2, \quad (43)$$

respectively, where the normalization constant Z is given in Eq. (D.17). Please see Eqs. (D.20) and (D.22) in the Appendix D.3 for the explicit expression of the integrals in Eqs. (42) and (43) respectively.

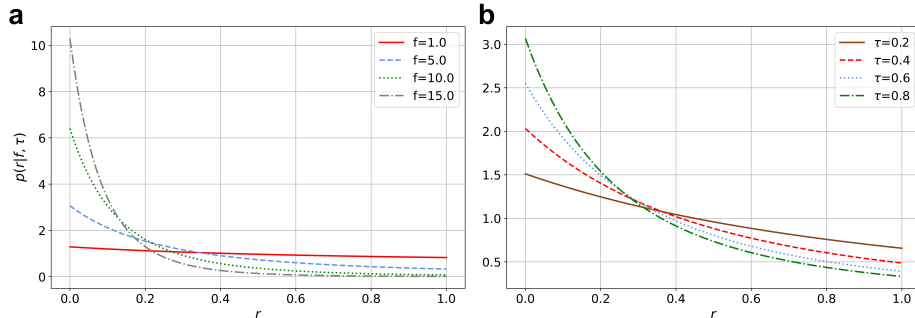


Figure 2: The shifted-geometric exponential PDF. **a** The PDFs for different values of f ($\tau = 0.8$). **b** The PDFs for different values of τ ($f = 5$).

4.0.1. Properties of the distributions

Sparsity

Figures 1 and 2 show that the sparsity for both the polylogarithmic exponential and the shifted-geometric exponential densities is controlled non-linearly by the f parameter. The densities with small values of f approach a uniform distribution, while the densities with large f values become very sparse. We can confirm this in the following limits for both distributions

$$\lim_{f \rightarrow 0} p(r|\boldsymbol{\lambda}) = \frac{e^0}{\int_0^1 e^0 dr'} = 1. \quad (44)$$

On the other extreme, as $f \rightarrow \infty$ both distributions tend to a Dirac delta distribution centered at 0 (Eq. (45)) (see Appendix D.6 for the proof).

$$\lim_{f \rightarrow \infty} p(r|\boldsymbol{\lambda}) = \delta(r). \quad (45)$$

which can be interpreted as a super-sparse distribution concentrated at 0. Compared to the polylogarithmic exponential distribution, the shifted-geometric exponential distribution exhibits fatter tails due to a slower decay in probability for increasing values of the population rate (See $f \in \{10, 15\}$ in Figs. 1a and 2a).

The m parameter also modulates sparsity for the polylogarithmic exponential distribution (Fig. 1b) but to a much lesser extent than the f parameter, i.e., the distribution is less sensitive to changes in the m parameter. Because of this, choosing $m = 1$, a case for which we provide the complete analytical PDF and distribution function, is the simplest choice of the polylogarithmic exponential distribution. Similarly, for the shifted-geometric exponential distribution, the τ parameter is less relevant for inducing sparsity (Fig. 2b) compared to the f parameter, but more when compared to the m polylogarithmic parameter.

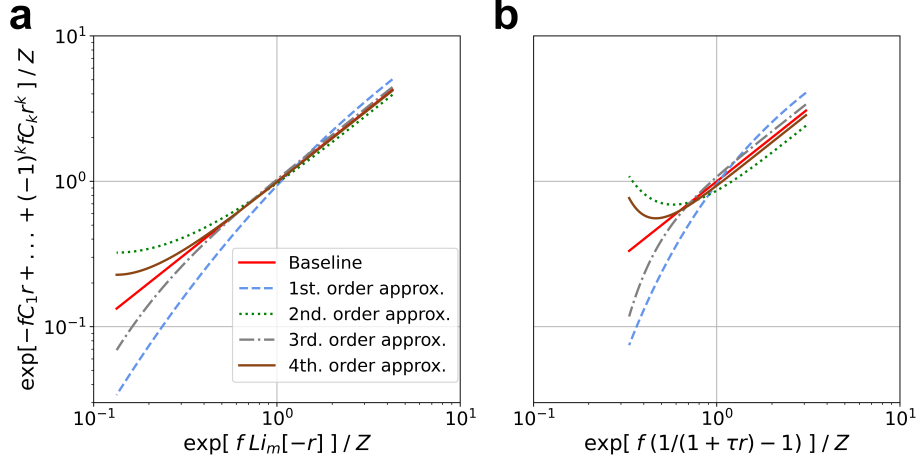


Figure 3: Comparison of the PDFs of the proposed models vs its approximation including up to the k -th order HOIs. **a** The polylogarithmic exponential PDF approximations with $m = 1$. The baseline is a red diagonal line. **b** The shifted-geometric exponential PDF approximations with $\tau = 0.8$. In all plots, $f = 5$.

Effect of HOIs

We assess the effect of HOIs in shaping the distributions by comparing the model with the argument of the exponent in the right-hand side of Eq. (32) truncated at the k -th order term against the original model. Figure 3 compares the polylogarithmic exponential PDF and the shifted-geometric exponential PDF in the log-log plot. In both PDFs, all of the k -th order approximations overall approximate better the ground truth values for larger r (i.e., smaller probability density) compared to the region near $r = 0$, where most neurons in the underlying population remain silent. In addition, the k -th order approximation alternates around the diagonal line (baseline) depending on whether k is even or odd, indicating overestimation and underestimation of the low probability densities, respectively, while this relation reverses for the approximation of the high probability densities. The approximated PDF becomes closer to the original model with increasing k (Fig. 3). Overall, the shifted-geometric exponential PDF exhibits more significant deviation even at the region of large probability density (small r , silent states) if we consider only the low order interactions (Fig. 3b), compared to the polylogarithmic exponential PDF (Fig. 3a). Thus, for the shifted-geometric exponential PDF, the HOIs shape not only the tail of the distribution but also the probabilities of silence.

Entropy and heat capacity

Here we assess the entropy and heat capacity of the distributions. First, the

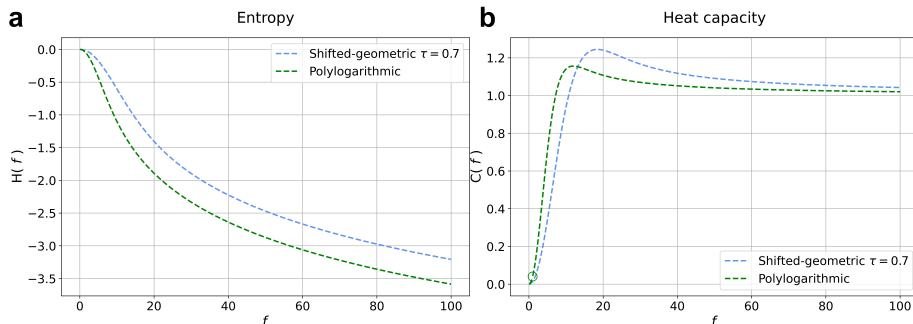


Figure 4: Entropy and heat capacity of the polylogarithmic exponential and the shifted-geometric exponential distributions. **a** Entropy of both distributions as f varies ($m = 1$, $\tau = 0.7$). **b** Heat capacity of both distributions as f varies ($m = 1$, $\tau = 0.7$). Notice the empty point at $f = 1$ for the heat capacity of the polylogarithmic model, where it is undetermined.

entropy of both distributions is computed as

$$\mathbb{E}_R [-\log(p(r|\boldsymbol{\lambda}))] = -\int_0^1 p(r|\boldsymbol{\lambda}) \log(p(r|\boldsymbol{\lambda})) dr. \quad (46)$$

For the explicit entropy of the polylogarithmic exponential and the shifted-geometric exponential distributions, see Appendix D.4.

Second, the heat capacity is computed as follows. Let $f = \frac{1}{T}$ and $df = -\frac{1}{T^2} dT$, where T denotes a temperature parameter. Then, the heat capacity of both the polylogarithmic exponential distribution (with $m = 1$) and the shifted-geometric distribution is computed as

$$C(f) = \frac{\partial}{\partial T} \left(-\frac{1}{Z} \frac{dZ}{df} \right) = f^2 \frac{d^2 Z}{df^2} \frac{1}{Z} - \frac{f^2}{Z^2} \left(\frac{dZ}{df} \right)^2. \quad (47)$$

See Appendix D.5 for the specific values of the normalization constant and its derivatives for the heat capacity of the polylogarithmic exponential and the shifted-geometric exponential distributions, as well as some limits with respect to f .

The entropy of the polylogarithmic exponential distribution ($m = 1$) is non-positive and a decreasing function of f as can be seen in Fig. 4a. Such negative entropy is compatible with a neural system that promotes a high level of organization. On the other hand, the heat capacity increases with f until a numerically found maximum at $f \approx 11.96$, after which it decreases until $\lim_{f \rightarrow \infty} C(f) = 1$ (see Appendix D.5). Such a limit can be intuitively observed in Fig. 4b. At $f = 1$, the heat capacity is undetermined (represented by an open circle in Fig. 4b for $m = 1$).

The entropy for the shifted-geometric exponential distribution is also non-positive and a decreasing function of f , compatible with a high level of organization, as can be seen in Fig. 4a for $\tau = 0.7$. The heat capacity (for $\tau = 0.7$)

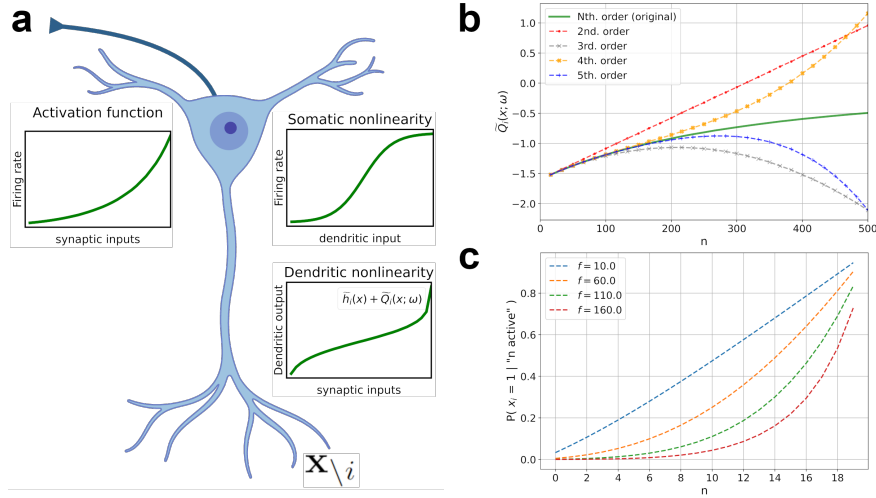


Figure 5: Neural interpretation of the alternating and shrinking HOIs models. **a** A schematic of a neuron i with somatic and dendritic nonlinearity of the shifted-geometric exponential distribution. (Top left) A nonlinear activation function of the neuron i that relates the output firing rate and synaptic inputs from the other neurons ($\mathbf{x}_{\setminus i}$). (Top right) A somatic activation function (logistic function), receiving the output of the dendritic activity as input. (Bottom right) Dendritic nonlinearity receiving inputs from presynaptic neurons $\mathbf{x}_{\setminus i}$. Created with *BioRender.com*. **b** The component of dendritic nonlinearity \bar{Q}_i for neuron i of the shifted-geometric exponential distribution for $\tau = 0.8$ as a function of the number of active input neurons, n , in a population of $N = 500$ neurons for a fixed value of $f = 2N$ (solid green). The dashed lines are the functions truncated at the second, third, fourth, and fifth-order interactions. **c** The activation functions of a neuron in a recurrent network composed of $N = 20$ neurons for different sparsity parameters. The activation function is the probability of activating the i th neuron given n active input neurons.

has a numerical maximum at $f \approx 18.44$ (Fig. 4b), after which it decreases until $C(f) \approx 1$. However, unlike the polylogarithmic exponential distribution ($m = 1$), we obtain that $\lim_{f \rightarrow \infty} C(f)$ is undetermined.

4.1. Neural Interpretation

The sampling dynamics to realize the joint distribution of the binary population activity, such as the Gibbs sampler (a.k.a Glauber dynamics), can be identified with the dynamics of recurrent neural networks. In such dynamics, each neuron responds to the inputs from the rest of the neurons with a specific nonlinear activation function. In this approach, the activity of an individual neuron is sampled from the conditional probability given the activities of the other neurons, either sequentially or in random order. The activity rate of the i th neuron is obtained as the following logistic function (see Appendix C.4 for

the details)

$$\mathcal{P}(x_i = 1 | \mathbf{x}_{\setminus i}, \boldsymbol{\omega}) = \frac{1}{1 + \exp\left(\left[-\log \frac{\mathcal{P}(x_i=1|\mathbf{x}_{\setminus i}, \boldsymbol{\omega})}{\mathcal{P}(x_i=0|\mathbf{x}_{\setminus i}, \boldsymbol{\omega})}\right]\right)}, \quad (48)$$

where the log ratio is computed as

$$\log\left(\frac{\mathcal{P}(x_i = 1 | \mathbf{x}_{\setminus i}, \boldsymbol{\omega})}{\mathcal{P}(x_i = 0 | \mathbf{x}_{\setminus i}, \boldsymbol{\omega})}\right) = \tilde{h}_i(\mathbf{x}) + \tilde{Q}_i(\mathbf{x}; \boldsymbol{\omega}), \quad (49)$$

Here, for the alternating and shrinking HOIs model, $\tilde{h}_i(\cdot)$ and $\tilde{Q}_i(\cdot)$ are given as

$$\tilde{h}_i(\mathbf{x}) = \log\left(\frac{1 + \sum_{j \neq i} x_j}{N - \sum_{j \neq i} x_j}\right) \quad (50)$$

and

$$\begin{aligned} & \tilde{Q}_i(\mathbf{x}; \boldsymbol{\omega}) \\ &= -f\left(\sum_{j=1}^N (-1)^{j+1} C_j \left(\frac{1 + \sum_{k \neq i} x_k}{N}\right)^j - \sum_{j=1}^N (-1)^{j+1} C_j \left(\frac{\sum_{k \neq i} x_k}{N}\right)^j\right). \end{aligned} \quad (51)$$

One can regard the logistic function as a somatic activation function of a neuron and the log ratio as a nonlinearity over synaptic inputs from other neurons at the dendrites (Fig. 5a), though other explanations could also apply. Note that $\tilde{h}_i(\mathbf{x})$ and $\tilde{Q}_i(\mathbf{x}; \boldsymbol{\omega})$ include the higher-order terms with respect to \mathbf{x} , indicating that the neuron is sensitive to higher-order statistics of input activities. This result contrasts with the Gibbs sampler of the pairwise maximum entropy model, resulting in the log-ratio given by the first-order terms with respect to \mathbf{x} . In this case, the neurons are sensitive only to the individual activities of the presynaptic neurons.

Both $\tilde{h}_i(\mathbf{x})$ and $\tilde{Q}_i(\mathbf{x}; \boldsymbol{\omega})$ are increasing functions with respect to the number of active neurons in the population, $\sum_i x_i$ (see the sum of their profile at the diagram in Fig. 5a). In particular, $\tilde{Q}_i(\mathbf{x}; \boldsymbol{\omega})$ is a sub-linear function with respect to the number of active input neurons, in contrast to the linear function expected for the neurons under the homogeneous pairwise (second-order) model (Fig. 5b). The even and odd order attenuate and promote the effect of sublinearity, respectively, resulting in the alternating convergence to $\tilde{Q}_i(\cdot)$ by adding higher-order terms.

The final input-output relation of the neurons caused by both the dendritic nonlinearity and somatic logistic activation function can be calculated as follows. Let n be the number of active presynaptic neurons for a neuron i . Then the

probability that the postsynaptic neuron i is activated is given as (see Appendix C.4 for the derivation)

$$\mathcal{P} \left(x_i = 1 \left| \sum_{j \neq i} x_j = n \right. \right) = \frac{1}{1 + \exp \left[\log \frac{N-n}{n+1} + \theta_{n+1} - \sum_{k=1}^n \theta_k \binom{n}{k-1} \right]}. \quad (52)$$

Figure 5c shows the conditional probability (Eq. (52)) as a function of n for the shifted-geometric exponential distribution. The spiking probability is facilitated by a larger number of active presynaptic neurons in a strictly increasing manner. However, the sparsity parameter f modifies this activation function nonlinearly. With larger f , the conditional probability of the activation is significantly attenuated for small n due to the sublinear property of $\tilde{Q}_i(\cdot)$ at small $n (\ll N)$. In contrast, this probability is kept high for larger n due to the diverging property of $\tilde{h}_i(\cdot)$ at large $n (\sim N)$, endowing the activation function with the property akin to the threshold nonlinearity. Such activation function with large f is expected to induce sparse population activity because the hyperactive state of the population becomes highly improbable, making the neurons silent most of the time.

4.2. Experimental data fitting

Here, we assess the goodness of fit of the proposed models to empirical data of parallel spike sequences recorded from in-vitro activities of salamander retinal ganglion cells [37]. The fitting procedure is as follows. We constructed the binarized salamander datasets using a 100 millisecond (ms) time window for the two datasets under different stimuli. We then extracted N_s samples $\mathbf{x}^{(i)}$, $i = 1, 2, \dots, N_s$, each composed of population activity of N retinal ganglion cells under a particular visual stimuli condition. We then transformed them into population rate samples. That is, we obtained $r_N^{(i)} \in [0, 1]$ where $r_N^{(i)} = \frac{1}{N} \sum_{k=1}^N x_k^{(i)}$ for each sample. Then, using the following log-likelihood function for the PDFs from the models

$$\ell \left(\boldsymbol{\lambda}; \left\{ r_N^{(i)} \right\}_{i=1}^{N_s} \right) = \sum_{i=1}^{N_s} \log p \left(r_N^{(i)} \mid \boldsymbol{\lambda} \right), \quad (53)$$

we obtained the parameters fitted to the data under the maximum likelihood principle, i.e.,

$$\hat{\boldsymbol{\lambda}} = \underset{\boldsymbol{\lambda}}{\operatorname{argmax}} \left\{ \ell \left(\boldsymbol{\lambda}; \left\{ r_N^{(i)} \right\}_{i=1}^{N_s} \right) \right\}. \quad (54)$$

In addition to the polylogarithmic and shifted-geometric models, we fit the first and second-order homogeneous population rate models for comparison. For the first-order model, we used the PDF from Eq. (14), which corresponds to a

	First-order	Second-order	Poly-logarithmic	Shifted-geometric
Binary white noise checkerboard stimuli dataset	2.8622 $f = 62.83$	2.8732 $f_1 = -60.29,$ $f_2 = 5.58$	2.8777 $f = 63.94$ $m = 1$	2.9078 $f = 70.12$ $\tau = 0.75$
Grayscale natural movie stimuli dataset	2.8621 $f = 62.83$	2.8737 $f_1 = -60.29,$ $f_2 = 5.58$	2.8801 $f = 63.96$ $m = 1$	2.9111 $f = 69.1$ $\tau = 0.8$

Table 2: Cross-validated log-likelihood per sample of each fitted model to two datasets (the grayscale natural movie stimuli and the white noise checkerboard stimuli) from salamander ganglion cells’ (binary) responses to different visual stimuli. The binary spikes in both datasets were obtained using a time window of 100 ms. We selected the $N = 40$ most active cells from the 152 (natural movie) and 155 (checkerboard) total neurons. We trained the models using a training set of size $N_s = 80,000$ for each dataset. We then computed the cross-validated log-likelihood using a test sample of size $N_s = 20,000$ for each dataset. The value of the cross-validated log-likelihood per a test sample is shown in the table. To learn the sparsity-inducing parameter f (or f_1 and f_2 for the second-order model), we used a gradient ascent method with the best learning rate among the values $\{0.001, 0.005, 0.01, 0.05, 0.1\}$. A grid search was performed for the C_j values of the alternating series of the corresponding model. The search for m in the polylogarithmic model was performed in $\{1 + 2t\}_{t=0}^5$ and for τ in the shifted-geometric model in $\{0.1 + 0.05t\}_{t=0}^{18}$.

truncated exponential distribution, the simplest sparse homogeneous model. It serves as a reference baseline to determine if other distributions are heavy-tailed or not in this $[0, 1]$ compact support, similarly to how the exponential distribution is used to evaluate the heavy-tailedness of other distributions with support in \mathbb{R} . For the second-order model, we used the PDF from Eq. (16). By Eq. (54), we obtain either one or two parameters. These parameters are

$$\lambda^* \approx \begin{cases} \hat{f} & \text{for the first-order exp. distr.} \\ \hat{f}_1, \hat{f}_2 & \text{for the second-order exp. distr.} \\ \hat{f}, \hat{m} & \text{for the polylogarithmic exp. distr.} \\ \hat{f}, \hat{\tau} & \text{for the shifted-geometric exp. distr.} \end{cases} \quad (55)$$

We divided the two binarized salamander datasets into training and test data sets. After fitting the models to the training data sets, we compared the polylogarithmic and shifted-geometric models against the first and second-order homogeneous population rate models, using the likelihoods of the unseen test data sets. Table 2 presents the results of the optimal fit for each type of model. The data histogram for one of the salamander datasets and the fitted models are shown in Fig. 6 in linear and logarithmic scales. First, we observed that, without constraining the sign of f_1 and f_2 in the second-order model, a substantial negative value was derived for f_1 , with an order of magnitude smaller positive f_2 , thereby closely approximating the first-order model, as seen in Fig. 6. Nonetheless, the significance of the distribution’s tail and related higher-order interactions are highlighted by the superior performance of the shifted-geometric model in both datasets in Table 2. In contrast, the performance of the polylogarithmic

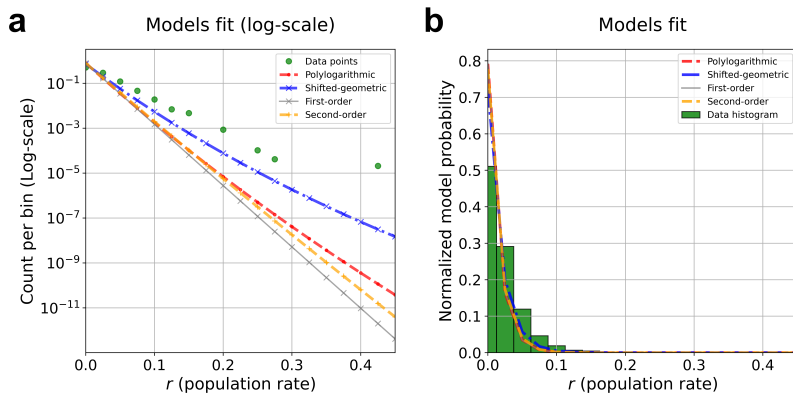


Figure 6: Models fitted to a binary dataset from salamander retinal ganglion cells responding to white noise checkerboard visual stimuli. **a** The fitted polylogarithmic (red) and shifted-geometric (blue) models to the data (green) in the logarithmic scale. In comparison, the plot shows the fitted first and second-order models. Each plot shows the best-fit curve in terms of average log-likelihood. **b** The same as in (a) in a linear scale for the vertical axis and the (original) dataset histogram.

model shows only marginal improvements over the first and second-order model in both datasets. The result indicates that the shifted-geometric model exhibits greater flexibility in capturing highly synchronous states that constitute the tail of the population spike-rate distributions.

5. Discussion

This study presented parametric models of distributions for the sparse collective activity of homogeneous binary neurons, inspired by the experimentally observed alternating HOIs. These distributions remain widespread with parameter-dependent sparsity in the limit of a large number of neurons. We derived these models by establishing sufficient conditions that ensure the PMF of the homogenous binary population results in a widespread continuous-valued population rate distribution in an infinitely large network.

The proposed models explain how a sparse, widespread distribution arises from specific HOIs with alternating shrinking structures. The models are consistent with a previous theoretical prediction by Amari et al. [26], which states that all orders of interactions are required to produce a widespread activity distribution in a large population of correlated neurons. However, here we showed that the base measure function, independently of the order of the (canonical) interactions, must be chosen carefully to avoid the dominance of the entropy term in the homogeneous distribution. We also showed that the proposed models outperformed the first and second-order interactions models when fitting to spiking data of salamander retinal ganglion cells responding to visual stimuli. In particular, the shifted-geometric exponential distribution improved the likelihood

of observing the data, underscoring the importance of the HOIs in capturing highly synchronized states with low probability because the shifted-geometric exponential distribution shows greater flexibility at its distribution tail.

Despite the prevalence of sparse, widespread distributions in neural systems, the mechanisms driving these patterns are still not fully understood and continue to be a subject of active investigation. One of the simplest yet insightful models that can reproduce these key features is the dichotomized Gaussian (DG) model [26, 13] and its extensions [38, 39, 40, 41, 42], which consists of threshold-neurons that become active if inputs sampled from a correlated multivariate Gaussian distribution exceed a threshold. The outputs of the DG neurons, represented as $(0, 1)$ patterns, exhibit sparse population activity [35, 16] with characteristic HOIs. Specifically, they display alternating signs in the interactions at successive orders, such as negative triplewise and positive quadruple-wise interactions and so on, with a shrinking magnitude [16, 41]. The structured HOIs contribute to the sparse activity and create the widespread distribution [26]. Supporting this theoretical prediction, the specific alternating structure of HOIs of up to the fifth order was found in neural population activity [16]. Furthermore, using more biologically plausible model neurons under the balanced inputs of excitatory and inhibitory neurons near the spiking threshold, it was discovered in [17] that the network architecture with excitatory shared (and hence correlated) inputs to pairs of neurons can explain the positive pairwise and negative triplewise interactions observed in monkey and mouse visual neurons while neurons receiving common inhibition can not. These results imply that the threshold nonlinearity of neurons, instead of the winner-all-take type network architecture, is a primary factor in inducing the observed sparsity.

The nonlinear functions derived from the convergence of the alternating shrinking HOI series are at the core of our models and fundamental for inducing the sparse and widespread population profile. We proposed two nonlinear functions, a logarithmic function and a function based on a shifted-geometric series, which are both strictly decreasing functions of the population rate. We consider that the nonlinearity driving the HOIs in neurons could originate from the combination of spiking nonlinearity at the soma and nonlinear dynamics at the dendrites. Dendritic computation, such as directional selectivity, coincidence detection in auditory neurons, temporal integration, image denoising, forward masking [43] and nonlinear integration of spatial cortical feedback in V1 neurons [44], exemplify the nonlinearity at dendrites. While modeling these nonlinearities opens up new avenues, sparsity is the main feature induced by the alternating and shrinking HOIs in this study. Indeed, the sparsity parameter nonlinearly modifies the input-output relationship of the neurons, endowing it with threshold nonlinearity that induces sparsity in the population activity. We note that both the structured HOIs and the base measure function introduced by this study contributed to constructing the threshold-like nonlinearity of the neurons, while the structured HOIs are involved in the sublinear integration of synaptic inputs (See also [19] for the sublinear integration induced by the negative triple-wise interactions and its optimality in coding natural scenes). As a support of the specific logarithmic computation, a modeling study on

collision-sensitive locust neurons suggests that their dendritic trees implement logarithmic transformations [45], which is supported by the fan-like dendritic structures identified in these neurons [45].

In light of the latest advances in machine learning that incorporate HOIs through specific nonlinearities of neurons [28, 29, 30, 31], we anticipate that significant steps forward in constructing energy-efficient computational machines will be gained by further deepening our understanding of the sparsity-inducing HOIs in neural dynamics through detailed mechanistic insights.

6. Acknowledgements

We thank Miguel Aguilera and Keito Wakatsuki for discussions and valuable comments on this manuscript. This work was supported by JSPS KAKENHI Grant Number JP 20K11709, 21H05246.

References

- [1] B. Willmore, D. J. Tolhurst, Characterizing the sparseness of neural codes, *Network: Computation in Neural Systems* 12 (3) (2001) 255.
- [2] B. Willmore, J. Mazer, J. Gallant, Sparse coding in striate and extrastriate visual cortex, *Journal of neurophysiology* 105 (6) (2011) 2907–2919.
- [3] W. E. Vinje, J. L. Gallant, Sparse coding and decorrelation in primary visual cortex during natural vision, *Science* 287 (5456) (2000) 1273–1276.
- [4] S. C. Yen, J. Baker, C. M. Gray, Heterogeneity in the responses of adjacent neurons to natural stimuli in cat striate cortex, *Journal of neurophysiology* 97 (2) (2007) 1326–1341.
- [5] E. Froudarakis, P. Berens, A. Ecker, R. Cotton, F. Sinz, D. Yatsenko, P. Saggau, M. Bethge, A. Tolias, Population code in mouse v1 facilitates readout of natural scenes through increased sparseness, *Nature neuroscience* 17 (6) (2014) 851–7.
- [6] B. A. Olshausen, D. J. Field, Sparse coding with an overcomplete basis set: A strategy employed by v1?, *Vision Research* 37 (23) (1997) 3311 – 3325.
- [7] E. Schneidman, M. J. Berry, R. Segev, W. Bialek, Weak pairwise correlations imply strongly correlated network states in a neural population, *Nature* 440 (2006) 1007–1012.
- [8] J. Shlens, G. D. Field, J. L. Gauthier, M. I. Grivich, D. Petrusca, A. Sher, A. M. Litke, E. J. Chichilnisky, The structure of multi-neuron firing patterns in primate retina, *Journal of Neuroscience* 26 (32) (2006) 8254–8266.
- [9] Y. Roudi, S. Nirenberg, P. E. Latham, Pairwise maximum entropy models for studying large biological systems: when they can work and when they can't, *PLoS computational biology* 5 (5) (2009) e1000380.

- [10] E. Ganmor, R. Segev, E. Schneidman, Sparse low-order interaction network underlies a highly correlated and learnable neural population code, *Proceedings of the National Academy of Sciences* 108 (23) (2011) 9679–9684.
- [11] G. Tkačik, O. Marre, D. Amodei, E. Schneidman, W. Bialek, M. J. Berry, II, Searching for collective behavior in a large network of sensory neurons, *PLOS Computational Biology* 10 (1) (2014) 1–23.
- [12] A. Barreiro, J. Gjorgjieva, F. Rieke, E. Shea-Brown, When do microcircuits produce beyond-pairwise correlations?, *Frontiers in Computational Neuroscience* 8 (2014).
- [13] S. Yu, H. Yang, H. Nakahara, G. S. Santos, D. Nikolić, D. Plenz, Higher-order interactions characterized in cortical activity, *Journal of Neuroscience* 31 (48) (2011) 17514–17526.
- [14] I. E. Ohiorhenuan, F. Mechler, K. P. Purpura, A. M. Schmid, Q. Hu, J. D. Victor, Sparse coding and high-order correlations in fine-scale cortical networks, *Nature* 466 (2010) 617–621.
- [15] F. Montani, R. A. Ince, R. Senatore, E. Arabzadeh, M. E. Diamond, S. Panzeri, The impact of high-order interactions on the rate of synchronous discharge and information transmission in somatosensory cortex, *Philosophical transactions. Series A, Mathematical, physical, and engineering sciences* 367 (1901) (2009) 3297–3310.
- [16] H. Shimazaki, K. Sadeghi, T. Ishikawa, Y. Ikegaya, T. Toyozumi, Simultaneous silence organizes structured higher-order interactions in neural populations, *Scientific Reports* 5 (9821) (2015).
- [17] S. R. Shomali, S. N. Rasuli, M. N. Ahmadabadi, H. Shimazaki, Uncovering hidden network architecture from spiking activities using an exact statistical input-output relation of neurons, *Communications Biology* 6 (1) (2023) 169.
- [18] N. A. Cayco-Gajic, J. Zylberberg, E. Shea-Brown, Triplet correlations among similarly tuned cells impact population coding, *Frontiers in Computational Neuroscience* 9 (2015).
- [19] J. Zylberberg, E. Shea-Brown, Input nonlinearities can shape beyond-pairwise correlations and improve information transmission by neural populations, *Phys. Rev. E* 92 (2015) 062707.
- [20] H. Shimazaki, S.-i. Amari, E. N. Brown, S. Grün, State-space analysis of time-varying higher-order spike correlation for multiple neural spike train data, *PLOS Computational Biology* 8 (3) (2012) 1–27.

- [21] G. Tkačik, T. Mora, O. Marre, D. Amodei, S. E. Palmer, M. J. Berry, W. Bialek, Thermodynamics and signatures of criticality in a network of neurons, *Proceedings of the National Academy of Sciences* 112 (37) (2015) 11508–11513.
- [22] M. Berry, D. Warland, M. Meister, The structure and precision of retinal spike trains, *Proceedings of the National Academy of Sciences of the United States of America* 94 (10) (1997) 5411–6.
- [23] O. Schwartz, J. Movellan, T. Wachtler, T. Albright, T. Sejnowski, Spike count distributions, factorizability, and contextual effects in area v1, *Neurocomputing* 58-60 (2004) 893–900.
- [24] D. Moshitch, I. Nelken, Using tweedie distributions for fitting spike count data, *Journal of Neuroscience Methods* 225 (2014) 13–28.
- [25] S. Chettih, C. Harvey, Single-neuron perturbations reveal feature-specific competition in v1, *Nature* 567 (2019) 334–340.
- [26] S.-I. Amari, H. Nakahara, S. Wu, Y. Sakai, Synchronous firing and higher-order interactions in neuron pool, *Neural computation* 15 (1) (2003) 127–42.
- [27] G. E. Hinton, R. R. Salakhutdinov, Reducing the dimensionality of data with neural networks, *science* 313 (5786) (2006) 504–507.
- [28] D. Krotov, J. J. Hopfield, Dense associative memory for pattern recognition, *Advances in neural information processing systems* 29 (2016).
- [29] F. Battiston, E. Amico, A. Barrat, G. Bianconi, G. Ferraz de Arruda, B. Franceschiello, I. Iacopini, S. Kéfi, V. Latora, Y. Moreno, et al., The physics of higher-order interactions in complex systems, *Nature Physics* 17 (10) (2021) 1093–1098.
- [30] H. Ramsauer, B. Schäfl, J. Lehner, P. Seidl, M. Widrich, T. Adler, L. Gruber, M. Holzleitner, M. Pavlović, G. K. Sandve, et al., Hopfield networks is all you need, *arXiv preprint arXiv:2008.02217* (2020).
- [31] L. Ambrogioni, In search of dispersed memories: Generative diffusion models are associative memory networks, *arXiv preprint arXiv:2309.17290* (2023).
- [32] L. Martignon, G. Deco, K. Laskey, M. Diamond, W. Freiwald, E. Vaadia, Neural coding: higher-order temporal patterns in the neurostatistics of cell assemblies, *Neural computation* 12 (11) (2000) 2621–2653.
- [33] H. Nakahara, S. Amari, Information-geometric measure for neural spikes, *Neural computation* 14 (10) (2002) 2269–2316.
- [34] A. Wohrer, M. Humphries, C. Machens, Population-wide distributions of neural activity during perceptual decision-making, *Progress in neurobiology* (2013) 156–93.

- [35] J. H. Macke, M. Opper, M. Bethge, Common input explains higher-order correlations and entropy in a simple model of neural population activity, *Physical review letters* 106 (20) (2011) 208102.
- [36] E. Masina, Useful review on the exponential-integral special function (2019). [arXiv:1907.12373](https://arxiv.org/abs/1907.12373).
- [37] A. R. Loback, G. Tkačik, J. S. Prentice, M. L. Ioffe, M. J. Berry II, O. Marre, M. J. Berry, Data from: Error-robust modes of the retinal population code [dataset], *dryad* (2017).
- [38] F. Montani, E. Phoka, M. Portesi, S. R. Schultz, Statistical modelling of higher-order correlations in pools of neural activity, *Physica A: Statistical Mechanics and its Applications* 392 (14) (2013) 3066–3086.
- [39] L. Montangie, F. Montani, Quantifying higher-order correlations in a neuronal pool, *Physica A: Statistical Mechanics and its Applications* 421 (2015) 388–400.
- [40] L. Montangie, F. Montani, Higher-order correlations in common input shapes the output spiking activity of a neural population, *Physica A: Statistical Mechanics and its Applications* 471 (2017) 845–861.
- [41] L. Montangie, F. Montani, Common inputs in subthreshold membrane potential: The role of quiescent states in neuronal activity, *Physical Review E* 97 (6) (2018) 060302.
- [42] D. Leen, E. Shea-Brown, A simple mechanism for beyond-pairwise correlations in integrate-and-fire neurons, *Journal of mathematical neuroscience* 5 (2015).
- [43] M. London, M. Häusser, Dendritic computation, *Annual Review of Neuroscience* 28 (1) (2005) 503–532, PMID: 16033324.
- [44] M. Fişek, D. Herrmann, A. Egea-Weiss, M. Cloves, L. Bauer, T.-Y. Lee, L. E. Russell, M. Häusser, Cortico-cortical feedback engages active dendrites in visual cortex, *Nature* (2023).
- [45] P. W. Jones, F. Gabbiani, Logarithmic compression of sensory signals within the dendritic tree of a collision-sensitive neuron, *The Journal of neuroscience: the official journal of the Society for Neuroscience* 32 (14) (2012) 4923–4934.

Alternating Shrinking Higher-order Interactions for Sparse Neural Population Activity

Supplementary Information

Ulises Rodríguez-Domínguez
rodriguezdominguez.ulises.2a@kyoto-u.ac.jp
Graduate School of Informatics, Kyoto University, Kyoto, Japan

Hideaki Shimazaki
h.shimazaki@i.kyoto-u.ac.jp
Graduate School of Informatics, Kyoto University, Kyoto, Japan
*Center for Human Nature, Artificial Intelligence, and Neuroscience (CHAIN),
Hokkaido University, Sapporo, Japan*

Appendix A. Homogeneous sparse population of neurons

Appendix A.1. Proof of Theorem 1

In the limit as $N \rightarrow \infty$, the homogeneous population rate distribution will become concentrated at r_N^0 if it converges to a delta peak at that location. For the PMF (5) to become a non-concentrated or widespread distribution, it must hold [26]

$$\lim_{N \rightarrow \infty} N [G_N(r_N; \boldsymbol{\theta}_N) - G_N(r_N^0; \boldsymbol{\theta}_N)] < \infty \quad (\text{A.1})$$

$$\forall r_N^0 \neq r_N \in S_r.$$

Because of the constant order of $NG_N(r_N; \boldsymbol{\theta}_N)$ (see Eq. (8)), we have

$$\mathcal{O}(NG_N(r_N; \boldsymbol{\theta}_N) - NG_N(r_N^0; \boldsymbol{\theta}_N)) = \mathcal{O}(1), \quad (\text{A.2})$$

and hence inequality (A.1) holds for $G_N(r_N; \boldsymbol{\theta}_N) < \infty$ with $r_N \in S_r$. This proves that (5) becomes widespread in the limit of $N \rightarrow \infty$.

On the other hand, recall $G_N(\cdot)$ is a non-positive strictly decreasing function with finite values in S_r . This means the maximum value for $G_N(r_N; \boldsymbol{\theta}_N)$ and also for the PMF (5) will be at $\inf\{S_r\} = \inf\{0, \frac{1}{N}, \frac{2}{N}, \dots, 1\} = 0$. Further, the maximum remains at 0 in the limit $\lim_{N \rightarrow \infty} \mathcal{P}(r_N | \boldsymbol{\theta}_N) = p(r | \boldsymbol{\lambda}) dr$ since $S_r \rightarrow [0, 1]$ as $N \rightarrow \infty$ and by continuity of the strictly decreasing property of $G_N(\cdot)$.

Appendix A.2. First-order homogeneous model

The distribution function corresponding to the PDF from Eq. (14) is

$$F(u|f) = \frac{1 - e^{-fu}}{1 - e^{-f}}. \quad (\text{A.3})$$

The mean is given by

$$\mu_R = \frac{1}{Z} \int_0^1 e^{-fr} r dr = \frac{1}{f(1-e^{-f})} - \frac{e^{-f}}{1-e^{-f}} \left(1 + \frac{1}{f}\right), \quad (\text{A.4})$$

and the variance is

$$\begin{aligned} \sigma_R^2 &= \frac{1}{Z} \int_0^1 e^{-fr} r^2 dr - \mu_R^2 \\ &= \frac{2}{f^2(1-e^{-f})} - \frac{e^{-f}}{1-e^{-f}} \left(\frac{2}{f^2} + \frac{2}{f}\right) - \frac{1}{f} e^{-f} - \mu_R^2. \end{aligned} \quad (\text{A.5})$$

Appendix B. Entropy-dominated homogeneous population

We now obtain Eq. (22). First, by using the Stirling formula with order notation (Eq. (21)) the logarithm of the binomial coefficient becomes

$$\begin{aligned}
\log \binom{N}{Nr_N} &= \log N! - \log (Nr_N)! - \log (N(1-r_N))! \\
&= \log \left(\sqrt{2\pi N} N^N e^{-N} \right) + \log \left(1 + \mathcal{O} \left(\frac{1}{N} \right) \right) \\
&\quad - \log \left(\sqrt{2\pi Nr_N} (Nr_N)^{Nr_N} e^{-Nr_N} \right) - \log \left(1 + \mathcal{O} \left(\frac{1}{Nr_N} \right) \right) \\
&\quad - \log \left(\sqrt{2\pi N(1-r_N)} (N(1-r_N))^{N(1-r_N)} e^{-N(1-r_N)} \right) \\
&\quad - \log \left(1 + \mathcal{O} \left(\frac{1}{N(1-r_N)} \right) \right) \\
&= -\log \left(\sqrt{2\pi Nr_N(1-r_N)} \right) + NH(r_N) + \mathcal{O} \left(\frac{1}{N} \left(1 - \frac{1}{1-r_N} - \frac{1}{r_N} \right) \right),
\end{aligned} \tag{B.1}$$

where the entropy term $H(r_N)$ is defined in Eq. (23). Since we consider $h(Nr_N) = 1$ for this case and given Eq. (B.1) the function $G_N(r_N; \theta_N)$ becomes

$$\begin{aligned}
G_N(r_N; \theta_N) &= \frac{1}{N} \log \binom{N}{Nr_N} + \frac{1}{N} Q_N(r_N; \theta_N) \\
&= -\frac{1}{N} \log \left(\sqrt{2\pi Nr_N(1-r_N)} \right) + H(r_N) + \frac{1}{N} Q_N(r_N; \theta_N) \\
&\quad + \frac{1}{N} \mathcal{O} \left(\frac{1}{N} \left(1 - \frac{1}{1-r_N} - \frac{1}{r_N} \right) \right).
\end{aligned} \tag{B.2}$$

The discrete support for the population rate can be partitioned into two sets where the $G_N(\cdot; \theta_N)$ function is either positive or non-positive as follows

$$r_N \in S_r^{G_N^+} \cup S_r^{G_N^-}, \tag{B.3}$$

where

$$S_r^{G_N^+} \equiv \{z_N \in S_r \mid G_N(r_N; \theta_N) > 0\}, \tag{B.4}$$

and

$$S_r^{G_N^-} \equiv \{z_N \in S_r \mid G_N(r_N; \theta_N) \leq 0\}. \tag{B.5}$$

The dominance of the entropy term seen in Eq. (24) for large values of N happens for $r_N \in S_r^{G_N^+}$. The fact that the entropy is non-negative and that it dominates over any non-positive term at a region allows the existence of the following maximizer

$$r_N^* = \operatorname{argmax}_{r_N \in S_r^{G_N^+} \cup S_r^{G_N^-}} \{G_N(r_N; \theta_N)\}$$

$$= \operatorname{argmax}_{r_N \in S_r^{G_N^+}} \{G_N(r_N; \boldsymbol{\theta}_N)\}, \quad (\text{B.6})$$

with $0 < r_N^* < 1$. Such a maximizer is strictly not at the extremes because the entropy vanishes there.

We now provide the limiting distribution for this entropy-dominated case. Recall that r denotes the continuous value that the random variable R takes.

We note that Eq. (5) can be rewritten by sending the numerator to the denominator and using the Kronecker notation as indicator function for each term in the PMF as

$$\begin{aligned} \mathcal{P}(r_N | \boldsymbol{\theta}_N) &= \sum_{r^j \in S_r} \frac{1}{\sum_{r' \in S_r} \exp[N(G_N(r'_N; \boldsymbol{\theta}_N) - G_N(r^j; \boldsymbol{\theta}_N))]} \delta_{r_N, r^j} \\ &= \sum_{r^j \in S_r} \frac{1}{\Xi(r^j; \boldsymbol{\theta}_N)} \delta_{r_N, r^j}. \end{aligned} \quad (\text{B.7})$$

Here, we can express the summation in each denominator (i.e., $\Xi(r_N; \boldsymbol{\theta}_N)$) by the disjoint parts as

$$\Xi(r_N; \boldsymbol{\theta}_N) = z^0 + z_N^+(r_N; \boldsymbol{\theta}_N) + z_N^-(r_N; \boldsymbol{\theta}_N), \quad (\text{B.8})$$

where

$$\begin{aligned} z^0 &= \exp[N(0)] = 1, \\ z_N^+(r_N; \boldsymbol{\theta}_N) &= \sum_{r'_N \in B_{r'}(r_N)^+} \exp[N((G_N(r'_N; \boldsymbol{\theta}_N) - G_N(r_N; \boldsymbol{\theta}_N))], \\ z_N^-(r_N; \boldsymbol{\theta}_N) &= \sum_{r'_N \in B_{r'}(r_N)^-} \exp[N(G_N(r'_N; \boldsymbol{\theta}_N) - G_N(r_N; \boldsymbol{\theta}_N))]. \end{aligned} \quad (\text{B.9})$$

with

$$B_{r'}(r_N)^+ \equiv \{r'_N | G_N(r'_N; \boldsymbol{\theta}_N) - G_N(r_N; \boldsymbol{\theta}_N) > 0\}. \quad (\text{B.10})$$

$$B_{r'}(r_N)^- \equiv \{r'_N | G_N(r'_N; \boldsymbol{\theta}_N) - G_N(r_N; \boldsymbol{\theta}_N) < 0\}. \quad (\text{B.11})$$

For the evaluation at the extremes of the support, we note that $G_N(r_N^*; \boldsymbol{\theta}_N) > G_N(r_N; \boldsymbol{\theta}_N) \quad \forall r_N \neq r_N^*$. In the limit we obtain for each denominator

$$\lim_{N \rightarrow \infty} \Xi(r_N^j; \boldsymbol{\theta}_N) \quad (\text{B.12})$$

$$= \begin{cases} z^0 + z_N^+(r_N; \boldsymbol{\theta}_N) + z_N^-(r_N; \boldsymbol{\theta}_N) = 1 + \infty + 0 & \text{if } r_N = 0 \\ z^0 + z_N^+(r_N; \boldsymbol{\theta}_N) + z_N^-(r_N; \boldsymbol{\theta}_N) = 1 + \infty + 0 & \text{if } r_N = 1 \\ z^0 + z_N^+(r_N; \boldsymbol{\theta}_N) + z_N^-(r_N; \boldsymbol{\theta}_N) = 1 + \infty + 0 & \text{if } r_N \neq 0, r_N \neq 1, \\ & r_N \neq r_N^* \\ z^0 + z_N^-(r_N; \boldsymbol{\theta}_N) = 1 + 0 & \text{if } r_N = r_N^*, \end{cases} \quad (\text{B.13})$$

where $r_N^* \rightarrow r^*$ for sufficiently large N . Then, the evaluation of the PMF at each of those points in the limit becomes

$$\lim_{N \rightarrow \infty} \mathcal{P}(r_N | \boldsymbol{\theta}_N) = \begin{cases} \frac{1}{\infty} \delta(r) & = 0 & \text{if } r_N = 0 \\ \frac{1}{\infty} \delta(r-1) & = 0 & \text{if } r_N = 1 \\ \frac{1}{\infty} \delta(0) & = 0 & \text{if } r_N \neq 0, r_N \neq 1, \\ & & r_N \neq r_N^* \\ \delta(r-r^*) & = +\infty & \text{if } r_N = r_N^* \end{cases} \quad (\text{B.14})$$

Hence, by combining the four cases for r_N , we obtain in the limit that the PDF is zero everywhere except at r^* where it tends to infinity, which corresponds to the delta PDF in Eq. (25) and the distribution function in Eq. (26).

Appendix C. The model with alternating and shrinking higher-order interactions

Appendix C.1. Canonical coordinates

The sum of total binary activity elevated to a given power $k > 0$ and $k \leq N$ can be expanded as follows (using the Multinomial Theorem),

$$\begin{aligned} \left(\sum_{i=1}^N x_i \right)^k &= \sum_{i=1}^N x_i^k + \sum_{i_1 < i_2} \sum_{k_{i_1} + k_{i_2} = k} \binom{k}{k_{i_1}, k_{i_2}} x_{i_1}^{k_{i_1}} x_{i_2}^{k_{i_2}} \\ &+ \sum_{i_1 < i_2 < i_3} \sum_{k_{i_1} + k_{i_2} + k_{i_3} = k} \binom{k}{k_{i_1}, k_{i_2}, k_{i_3}} x_{i_1}^{k_{i_1}} x_{i_2}^{k_{i_2}} x_{i_3}^{k_{i_3}} \\ &+ \dots + \sum_{i_1 < i_2 < \dots < i_k} k! x_{i_1} x_{i_2} \dots x_{i_k}, \end{aligned} \quad (\text{C.1})$$

where $\binom{k}{k_{i_1}, k_{i_2}, \dots, k_{i_N}} = \frac{k!}{k_{i_1}! k_{i_2}! \dots k_{i_N}!}$ is a multinomial coefficient with $k_{i_1} > 0, k_{i_2} > 0, \dots, k_{i_N} > 0$. Using the fact that any x_i is binary, the powers of x_i in Eq. (C.1) reduce as follows

$$\begin{aligned} \left(\sum_{i=1}^N x_i \right)^k &= \sum_{i=1}^N x_i + \sum_{i_1 < i_2} \sum_{k_{i_1} + k_{i_2} = k} \binom{k}{k_{i_1}, k_{i_2}} x_{i_1} x_{i_2} + \dots + \\ &+ \sum_{i_1 < i_2 < i_3} \sum_{k_{i_1} + k_{i_2} + k_{i_3} = k} \binom{k}{k_{i_1}, k_{i_2}, k_{i_3}} x_{i_1} x_{i_2} x_{i_3} \\ &+ \dots + \sum_{i_1 < i_2 < \dots < i_k} k! x_{i_1} x_{i_2} \dots x_{i_k}. \end{aligned} \quad (\text{C.2})$$

Following the multinomial expansion from Eq. (C.2), the canonical form of our binary PMF can be obtained as

$$\begin{aligned} \mathcal{P}(\mathbf{x}|\boldsymbol{\omega}) &= \frac{h(\mathbf{x})}{Z} \exp \left[-f \sum_{j=1}^N (-1)^{j+1} C_j \left(\frac{\sum_{i=1}^N x_i}{N} \right)^j \right] \\ &= \frac{h(\mathbf{x})}{Z} \exp \left[-f \left(C_1 \frac{\sum_{i=1}^N x_i}{N} - C_2 \frac{\left(\sum_{i=1}^N x_i \right)^2}{N^2} \right. \right. \\ &\quad \left. \left. + \dots + (-1)^{N+1} C_N \frac{\left(\sum_{i=1}^N x_i \right)^N}{N^N} \right) \right] \\ &= \frac{h(\mathbf{x})}{Z} \exp \left[-\frac{f C_1}{N} \sum_{i=1}^N x_i \right] \end{aligned}$$

$$\begin{aligned}
& + \frac{fC_2}{N^2} \left(\sum_{i=1}^N x_i \right)^2 \\
& - \frac{fC_3}{N^3} \left(\sum_{i=1}^N x_i \right)^3 \\
& \vdots \\
& + (-1)^{N+1} \frac{fC_N}{N^N} \left(\sum_{i=1}^N x_i \right)^N \Big] \\
= & \frac{h(\mathbf{x})}{Z} \exp \left[-\frac{fC_1}{N} \sum_{i=1}^N x_i \right. \\
& + \frac{fC_2}{N^2} \left(\sum_{i=1}^N x_i + 2 \sum_{i_1 < i_2} x_{i_1} x_{i_2} \right) \\
& - \frac{fC_3}{N^3} \left(\sum_{i=1}^N x_i + 6 \sum_{i_1 < i_2} x_{i_1} x_{i_2} + 6 \sum_{i_1 < i_2 < i_3} x_{i_1} x_{i_2} x_{i_3} \right) \\
& \vdots \\
& \left. + (-1)^{N+1} \frac{fC_N}{N^N} \left(\sum_{i=1}^N x_i + \sum_{i_1 < i_2} \sum_{k_1+k_2=N} \binom{N}{k_1, k_2} x_{i_1} x_{i_2} \right. \right. \\
& \qquad \qquad \qquad \left. \left. + \dots + N! x_{i_1} x_{i_2} \dots x_{i_N} \right) \right] \tag{C.3}
\end{aligned}$$

Here, we compare the above equation with the canonical form of the exponential family distribution:

$$\mathcal{P}(\mathbf{x}|\boldsymbol{\theta}_N) = \frac{h(\mathbf{x})}{Z} \exp \left[\theta_1 \sum_{i=1}^N x_i + \theta_2 \sum_{i_1 < i_2} x_{i_1} x_{i_2} + \dots + \theta_N x_{i_1} x_{i_2} \dots x_{i_N} \right], \tag{C.4}$$

where $h(\mathbf{x})$ is defined as in Eq. (9). The canonical parameter $\boldsymbol{\theta}_N$ is obtained by grouping the coefficients that multiply every power function of the coordinates in \mathbf{x} , i.e.,

$$\begin{aligned}
\theta_1 &= \sum_{l=1}^N (-1)^l \frac{fC_l}{N^l}, \\
\theta_2 &= \sum_{l=2}^N (-1)^l \frac{fC_l}{N^l} \sum_{k_1+k_2=l} \binom{l}{k_1, k_2},
\end{aligned}$$

$$\begin{aligned} & \vdots \\ \theta_N &= (-1)^N \frac{f_{C_N}}{N^N} N!. \end{aligned} \quad (\text{C.5})$$

Appendix C.2. Population rate probability density function

We now show the proof to obtain our limiting alternating PDF from Eq. (32). For the remainder of the homogeneous analysis we make use of Stirling numbers of the first kind, which are defined as follows for $m > 0$

$$s(k, m) = (-1)^{k-m} \left[\begin{matrix} k \\ m \end{matrix} \right], \quad (\text{C.6})$$

where

$$\left[\begin{matrix} k \\ m \end{matrix} \right] = (k-1) \left[\begin{matrix} k-1 \\ m \end{matrix} \right] + \left[\begin{matrix} k-1 \\ m-1 \end{matrix} \right], \quad (\text{C.7})$$

with the initial conditions (for $k > 0$)

$$\left[\begin{matrix} 0 \\ 0 \end{matrix} \right] = 1, \quad \left[\begin{matrix} k \\ 0 \end{matrix} \right] = \left[\begin{matrix} 0 \\ k \end{matrix} \right] = 0, \quad (\text{C.8})$$

and the identity

$$\left[\begin{matrix} k \\ k \end{matrix} \right] = 1. \quad (\text{C.9})$$

Stirling numbers of the first kind are useful to rewrite the binomial coefficients in an expanded polynomial form as follows

$$\binom{n}{k} = \frac{1}{k!} \sum_{m=0}^k s(k, m) n^m. \quad (\text{C.10})$$

The polynomial term in the exponential argument of our alternating PMF is

$$\begin{aligned} Q_N(r_N; \theta_N) &= \sum_{k=1}^{Nr_N} \binom{Nr_N}{k} \theta_k \\ &= \sum_{k=1}^{Nr_N} \frac{1}{k!} \sum_{m=0}^k s(k, m) (Nr_N)^m \theta_k \\ &= \sum_{k=1}^{Nr_N} \theta_k \sum_{m=0}^k (-1)^{k-m} \left[\begin{matrix} k \\ m \end{matrix} \right] \frac{(Nr_N)^m}{k!} \\ &= \sum_{k=1}^{Nr_N} \theta_k \left[(-1)^k \left[\begin{matrix} k \\ 0 \end{matrix} \right] \frac{(Nr_N)^0}{k!} + (-1)^0 \left[\begin{matrix} k \\ k \end{matrix} \right] \frac{(Nr_N)^k}{k!} + \right. \end{aligned}$$

$$\begin{aligned}
& \sum_{m=1}^{k-1} (-1)^{k-m} \binom{k}{m} \frac{(Nr_N)^m}{k!} \\
= & \sum_{k=1}^{Nr_N} \theta_k \left[\frac{(Nr_N)^k}{k!} \right] + \sum_{k=1}^{Nr_N} \theta_k \left[\sum_{m=1}^{k-1} (-1)^{k-m} \binom{k}{m} \frac{(Nr_N)^m}{k!} \right],
\end{aligned} \tag{C.11}$$

where the later was obtained using the identities Eqs. (C.8) and (C.9). The first term in the last right-hand side of Eq. (C.11) can be expanded as

$$\begin{aligned}
\sum_{k=1}^{Nr_N} \theta_k \left[\frac{(Nr_N)^k}{k!} \right] &= \sum_{l=1}^N (-1)^l f \frac{C_l}{N^l} (Nr_N) \\
&+ \sum_{l=2}^N (-1)^l f \frac{C_l}{N^l} \sum_{k_1+k_2=l} \binom{l}{k_1, k_2} \frac{(Nr_N)^2}{2!} \\
&+ \dots \\
&+ \sum_{l=Nr_N}^N (-1)^l f \frac{C_l}{N^l} \sum_{k_1+\dots+k_{Nr_N}=l} \binom{l}{k_1, \dots, k_{Nr_N}} \frac{(Nr_N)^{Nr_N}}{(Nr_N)!} \\
= & (-1)^1 f \frac{C_1}{N^1} Nr_N + \sum_{l=2}^N (-1)^l f \frac{C_l}{N^l} Nr_N \\
&+ (-1)^2 f \frac{C_2 2! N^2 (r_N)^2}{N^2 2!} + \sum_{l=3}^N (-1)^l f \frac{C_l}{N^l} \sum_{k_1+k_2=l} \binom{l}{k_1, k_2} \frac{(Nr_N)^2}{2!} \\
&+ \dots \\
&+ (-1)^{Nr_N} f \frac{C_{Nr_N} (Nr_N)! N^{Nr_N} r^{Nr_N}}{N^{Nr_N} (Nr_N)!} \\
&+ \sum_{l=Nr_N+1}^N (-1)^l f \frac{C_l}{N^l} \sum_{k_1+\dots+k_{Nr_N}=l} \binom{l}{k_1, \dots, k_{Nr_N}} \frac{N^{Nr_N} (r_N)^{Nr_N}}{(Nr_N)!} \\
= & \sum_{j=1}^{Nr_N} (-1)^j f \frac{C_j}{N^j} N^j (r_N)^j + \mathcal{O}\left(\frac{1}{N}\right) \\
= & \sum_{j=1}^{Nr_N} (-1)^j f C_j (r_N)^j + \mathcal{O}\left(\frac{1}{N}\right) \\
= & -f \sum_{j=1}^{Nr_N} (-1)^{j+1} C_j (r_N)^j + \mathcal{O}\left(\frac{1}{N}\right).
\end{aligned} \tag{C.12}$$

On the other hand, we can obtain the order for the second term in the last

right-hand side of Eq. (C.11) as follows

$$\begin{aligned}
& \mathcal{O} \left(\sum_{k=1}^{Nr_N} \theta_k \left[\sum_{m=1}^{k-1} (-1)^{k-m} \begin{bmatrix} k \\ m \end{bmatrix} \frac{N^m (r_N)^m}{k!} \right] \right) \\
&= \mathcal{O} \left(\theta_1 + \theta_2 (-1) \begin{bmatrix} 2 \\ 1 \end{bmatrix} \frac{N^1 (r_N)^1}{2!} + \right. \\
&\quad \left. + \dots + \theta_{Nr_N} \sum_{m=1}^{Nr_N-1} (-1)^{Nr_N-m} \begin{bmatrix} Nr_N \\ m \end{bmatrix} \frac{N^m (r_N)^m}{(Nr_N)!} \right), \quad (\text{C.13})
\end{aligned}$$

where the highest order for each θ_k corresponds to its first term (since its terms grow inversely in N). The order is then

$$\begin{aligned}
& \mathcal{O} \left(\sum_{k=1}^{Nr_N} \theta_k \left[\sum_{m=1}^{k-1} (-1)^{k-m} \begin{bmatrix} k \\ m \end{bmatrix} \frac{N^m (r_N)^m}{k!} \right] \right) \\
&= \mathcal{O} \left(\frac{1}{N} + \frac{1}{N^2} \frac{N}{2!} + \dots + \frac{1}{N^{Nr_N}} (Nr_N)! \frac{N^{Nr_N-1}}{(Nr_N)!} \right) \\
&= \mathcal{O} \left(\frac{1}{N} \right). \quad (\text{C.14})
\end{aligned}$$

Considering Eqs. (C.11), (C.12) and (C.14), the polynomial term can be written as in Eq. (31) and our PMF becomes

$$\mathcal{P}(r_N | \boldsymbol{\theta}_N) = \frac{1}{Z} \exp \left[-f \sum_{j=1}^{Nr_N} (-1)^{j+1} C_j (r_N)^j + \mathcal{O} \left(\frac{1}{N} \right) \right]. \quad (\text{C.15})$$

Appendix C.3. Widespread probability density function limit

Using Eq. (C.15) in the limit as $N \rightarrow \infty$ our PMF becomes

$$\begin{aligned}
\lim_{N \rightarrow \infty} \mathcal{P}(r_N | \boldsymbol{\theta}_N) &= \frac{1}{Z} \exp \left[-f \sum_{j=1}^{\infty} (-1)^{j+1} C_j r^j \right] dr \\
&= p(r | \boldsymbol{\lambda}) dr, \quad (\text{C.16})
\end{aligned}$$

where $\boldsymbol{\lambda} = \left\{ f, \{C_j\}_{j \in \mathbb{N}^+} \right\}$. The specific form of the distribution (C.16) and its convergence depends on the C_j constants. By Leibniz criterion for alternating series the following series in our alternating density

$$-f \sum_{j=1}^{\infty} (-1)^{j+1} C_j r^j = f \sum_{j=1}^{\infty} (-1)^j C_j r^j \quad (\text{C.17})$$

converge if the following conditions hold:

$$\begin{aligned} |C_1 r| > |C_2 r^2| > |C_3 r^3| > \dots, \\ \lim_{j \rightarrow \infty} [C_j r^j] = 0. \end{aligned} \quad (\text{C.18})$$

The conditions in Eq. (C.18) hold for the following cases but are not restricted to them.

Polylogarithmic exponential PDF

If we define $C_j = \frac{1}{j^m} \forall j$ then the PDF in (C.16) is as in Eq. (33), where $\text{Li}_m[\cdot]$ is the polylogarithm function of order $m = 1, 2, 3, \dots$, defined as

$$\text{Li}_m [x] = \sum_{j=1}^{\infty} \frac{x^j}{j^m} \quad (\text{C.19})$$

When $m = 1$, the series converges to the natural logarithm, i.e., Eq. (34).

Shifted-geometric exponential PDF

If we instead define $C_j = (\tau)^j$, with $0 < \tau < 1, \forall j$ so that $\tau r < 1$ then the distribution in (C.16) is as in Eq. (39). To see why Eq. (39) holds, we consider the following

$$\begin{aligned} \lim_{n \rightarrow \infty} \left[-f \sum_{j=1}^n (-1)^{j+1} (\tau r)^j \right] &= f \lim_{n \rightarrow \infty} \left[\sum_{j=1}^n (-1)^j (\tau r)^j \right] \\ &= f \lim_{n \rightarrow \infty} \left[\sum_{j=1}^n (-\tau r)^j \right] \\ &= f \lim_{n \rightarrow \infty} \left[\frac{-\left(\tau r + (-1)^{n+1} (\tau r)^{n+1}\right)}{1 + \tau r} \right] \\ &= -f \frac{1}{1 + \frac{1}{\tau r}} \\ &= f \left(\frac{1}{1 + \tau r} - 1 \right). \end{aligned} \quad (\text{C.20})$$

Appendix C.4. Neural interpretation

The conditional probability that the i th neuron spikes given the rest of the neurons in the population is derived as follows

$$\mathcal{P}(x_i = 1 | \mathbf{x}_{\setminus i}, \boldsymbol{\omega}) = \frac{\mathcal{P}(x_i = 1, \mathbf{x}_{\setminus i}, \boldsymbol{\omega})}{\mathcal{P}(\mathbf{x}_{\setminus i}, \boldsymbol{\omega})}$$

$$\begin{aligned}
&= \frac{\mathcal{P}(x_i = 1 | \mathbf{x}_{\setminus i}, \boldsymbol{\omega}) \mathcal{P}(\mathbf{x}_{\setminus i}, \boldsymbol{\omega})}{\mathcal{P}(x_i = 1 | \mathbf{x}_{\setminus i}, \boldsymbol{\omega}) \mathcal{P}(\mathbf{x}_{\setminus i}, \boldsymbol{\omega}) + \mathcal{P}(x_i = 0 | \mathbf{x}_{\setminus i}, \boldsymbol{\omega}) \mathcal{P}(\mathbf{x}_{\setminus i}, \boldsymbol{\omega})} \\
&= \frac{1}{1 + \frac{\mathcal{P}(x_i = 0 | \mathbf{x}_{\setminus i}, \boldsymbol{\omega})}{\mathcal{P}(x_i = 1 | \mathbf{x}_{\setminus i}, \boldsymbol{\omega})}} \\
&= \frac{1}{1 + \exp\left(\left[-\log \frac{\mathcal{P}(x_i = 1 | \mathbf{x}_{\setminus i}, \boldsymbol{\omega})}{\mathcal{P}(x_i = 0 | \mathbf{x}_{\setminus i}, \boldsymbol{\omega})}\right]\right)}. \tag{C.21}
\end{aligned}$$

The log ratio is obtained as

$$\begin{aligned}
&\log\left(\frac{\mathcal{P}(x_i = 1 | \mathbf{x}_{\setminus i}, \boldsymbol{\omega})}{\mathcal{P}(x_i = 0 | \mathbf{x}_{\setminus i}, \boldsymbol{\omega})}\right) \\
&= \log\left(\frac{h\left(1 + \sum_{j \neq i} x_j\right)}{Z} \exp\left[-f \sum_{j=1}^N (-1)^{j+1} C_j \left(\frac{1 + \sum_{k \neq i} x_k}{N}\right)^j\right]\right) \\
&\quad - \log\left(\frac{h\left(0 + \sum_{j \neq i} x_j\right)}{Z} \exp\left[-f \sum_{j=1}^N (-1)^{j+1} C_j \left(\frac{0 + \sum_{k \neq i} x_k}{N}\right)^j\right]\right) \\
&= \log\left(\frac{h\left(1 + \sum_{j \neq i} x_j\right)}{h\left(\sum_{j \neq i} x_j\right)}\right) \\
&\quad + \log\left(\exp\left[-f \sum_{j=1}^N (-1)^{j+1} C_j \left(\frac{1 + \sum_{k \neq i} x_k}{N}\right)^j\right]\right) \\
&\quad - \log\left(\exp\left[-f \sum_{j=1}^N (-1)^{j+1} C_j \left(\frac{\sum_{k \neq i} x_k}{N}\right)^j\right]\right) \\
&= \log\left(\frac{1 + \sum_{j \neq i} x_j}{N - \sum_{j \neq i} x_j}\right) \\
&\quad - f \left(\sum_{j=1}^N (-1)^{j+1} C_j \left(\frac{1 + \sum_{k \neq i} x_k}{N}\right)^j - \sum_{j=1}^N (-1)^{j+1} C_j \left(\frac{\sum_{k \neq i} x_k}{N}\right)^j\right) \\
&= \tilde{h}_i(\mathbf{x}) + \tilde{Q}_i(\mathbf{x}; \boldsymbol{\omega}), \tag{C.22}
\end{aligned}$$

where the simplified argument for the ratio between base measure function values comes from the following

$$\frac{h\left(1 + \sum_{j \neq i} x_j\right)}{h\left(\sum_{j \neq i} x_j\right)} = \frac{\binom{N}{\sum_{j \neq i} x_j}}{\binom{N}{1 + \sum_{j \neq i} x_j}}$$

$$\begin{aligned}
&= \frac{\frac{N!}{(\sum_{j \neq i} x_j)!(N - \sum_{j \neq i} x_j)!}}{\frac{N!}{(1 + \sum_{j \neq i} x_j)!(N - 1 - \sum_{j \neq i} x_j)!}} \\
&= \frac{(1 + \sum_{j \neq i} x_j) (\sum_{j \neq i} x_j)! (N - \sum_{j \neq i} x_j - 1)!}{(\sum_{j \neq i} x_j)! (N - \sum_{j \neq i} x_j) (N - \sum_{j \neq i} x_j - 1)!} \\
&= \frac{1 + \sum_{j \neq i} x_j}{N - \sum_{j \neq i} x_j}. \tag{C.23}
\end{aligned}$$

The derivation of Eq. (52) is as follows

$$\begin{aligned}
&\mathcal{P} \left(x_i = 1 \left| \sum_{j \neq i} x_j = n \right. \right) \\
&= \frac{\mathcal{P} \left(x_i = 1, \sum_{j \neq i} x_j = n \right)}{\mathcal{P} \left(\sum_{j \neq i} x_j = n \right)} \\
&= \frac{\binom{N-1}{n} \frac{h(1 + \sum_{j \neq i} x_j)}{Z} \exp \left[\sum_{k=1}^{n+1} \binom{n+1}{k} \theta_k \right]}{\sum_{s \in \{0,1\}} \binom{N-1}{n} \frac{h(s + \sum_{j \neq i} x_j)}{Z} \exp \left[\sum_{k=1}^{n+s} \binom{n+s}{k} \theta_k \right]} \\
&\quad \frac{\binom{N-1}{n} \frac{1}{\binom{N}{n+1}} \frac{1}{Z} \exp \left[\sum_{k=1}^{n+1} \binom{n+1}{k} \theta_k \right]}{\sum_{s \in \{0,1\}} \binom{N-1}{n} \frac{1}{\binom{N}{n+s}} \frac{1}{Z} \exp \left[\sum_{k=1}^{n+s} \binom{n+s}{k} \theta_k \right]} \\
&= \frac{(n+1) \exp \left[\sum_{k=1}^{n+1} \binom{n+1}{k} \theta_k \right]}{(n+1) \exp \left[\sum_{k=1}^{n+1} \binom{n+1}{k} \theta_k \right] + (N-n) \exp \left[\sum_{k=1}^n \binom{n}{k} \theta_k \right]} \\
&= \frac{1}{1 + \frac{N-n}{n+1} \exp \left[\sum_{k=1}^n \binom{n}{k} \theta_k - \sum_{k=1}^{n+1} \binom{n+1}{k} \theta_k \right]} \\
&= \frac{1}{1 + \exp \left[\log \frac{N-n}{n+1} + \theta_{n+1} + \sum_{k=1}^n \theta_k \left\{ \binom{n}{k} - \binom{n+1}{k} \right\} \right]}. \\
&= \frac{1}{1 + \exp \left[\log \frac{N-n}{n+1} + \theta_{n+1} - \sum_{k=1}^n \theta_k \binom{n}{k-1} \right]}, \tag{C.24}
\end{aligned}$$

where we used the Pascal's equality to obtain the last equality:

$$\binom{n}{k} + \binom{n}{k-1} = \binom{n+1}{k}. \quad (\text{C.25})$$

Appendix D. Properties of the polylogarithmic and shifted-geometric exponential densities

Appendix D.1. Non-positive property for the arguments of the exponential function

Polylogarithmic exponential density

For $m = 1$ we have the function

$$f\text{Li}_1[-r] = -f \log(1+r) \leq 0 \quad \forall r \in [0, 1] \quad (\text{D.1})$$

because $\log(x)$ is a strictly increasing function for $x > 0$ and correspondingly $-f \log(x)$ ($f > 0$) is a strictly decreasing function for $x > 0$, where $-f \log(1+r) = 0$ for $r = 0$ and $-f \log(1+r) = -f \log 2$ for $r = 1$. Then inequality (D.1) holds for $r \in [0, 1]$ and $-f \log(1+r)$ has a maximum at $r = 0$.

For $m \in \{2, 3, 4, \dots\}$ the following alternating series (shown on the right-hand side in parenthesis)

$$f\text{Li}_m[-r] = f \left(\sum_{j=1}^{\infty} \frac{(-r)^j}{j^m} \right) \quad (\text{D.2})$$

converge to a finite limit L by the Leibniz criterion. In this case, $L = \text{Li}_m[-r]$, and the convergence proof of the Leibniz criterion for alternating series guarantees the following bounds for any $n > 0$

$$S_{2n} \leq L \leq S_{2n+1}, \quad (\text{D.3})$$

where S_{2n} denotes the partial sum of an even number of terms and S_{2n+1} denotes the partial sum of an odd number of terms in the alternating series. Then we have the partial sum with an even number of terms ($2n = 2$)

$$\begin{aligned} S_2 &= \sum_{j=1}^2 \frac{(-r)^j}{j^m} \\ &= -r + \frac{r^2}{2^m} \leq 0 \quad \forall r \in [0, 1], \end{aligned} \quad (\text{D.4})$$

where the last inequality holds because the coefficient of the first negative term is such that $r \geq r^2 \geq \frac{r^2}{2^m} \quad \forall r \in [0, 1]$. Similarly, we have the following partial sum with an odd number of terms ($2n + 1 = 3$)

$$\begin{aligned} S_3 &= \sum_{j=1}^3 \frac{(-r)^j}{j^m} \\ &= S_2 - \frac{r^3}{3^m} \leq 0 \quad \forall r \in [0, 1], \end{aligned} \quad (\text{D.5})$$

where the last inequality holds because $S_2 \leq 0$ by inequality (D.4) and since $-\frac{r^3}{3^m} \leq 0$ for $r \in [0, 1]$. Using inequalities (D.3) and (D.5) we have for $m \in \{2, 3, 4, \dots\}$ that

$$\text{Li}_m[-r] \leq 0 \quad \forall r \in [0, 1] \quad (\text{D.6})$$

and also for $f > 0$ we have $f\text{Li}_m[-r] \leq 0$. Consequently by Eqs. (D.6) and (D.1) the function in Eq. (D.2) is non-positive for $r \in [0, 1]$ with $m \in \{1, 2, 3, \dots\}$.

Shifted-geometric exponential density

For the shifted-geometric function, we have the following inequality

$$f \left(\frac{1}{1+\tau r} - 1 \right) \leq 0 \quad \forall r \in [0, 1] \quad (\text{D.7})$$

because for $\tau > 0$ it holds that $\frac{1}{1+\tau r} \leq 1$ for $r \in [0, 1]$. Equality in Eq. (D.7) is reached only when $r = 0$ and hence $f \left(\frac{1}{1+\tau r} - 1 \right)$ is non-positive with a maximum at $r = 0$.

Appendix D.2. Decreasing property for the arguments of the exponential function

Polylogarithmic exponential density

We now prove the decreasing property for the polylogarithmic function in the polylogarithmic exponential density in Eq. (33). For $m = 1$, the derivative of the function is

$$\begin{aligned} \frac{d}{dr} [f\text{Li}_1[-r]] &= \frac{d}{dr} [-f \log(1+r)] \\ &= -\frac{f}{1+r} < 0 \quad \forall r \in [0, 1], \end{aligned} \quad (\text{D.8})$$

since $f > 0$. On the other hand, for $m \in \{2, 3, 4, \dots\}$ the derivative is

$$\begin{aligned} \frac{d}{dr} [f\text{Li}_m[-r]] &= f \frac{d}{dr} [\text{Li}_m[-r]] \\ &= f \left[\frac{1}{r} \text{Li}_{m-1}[-r] \right] \\ &= f \left[\sum_{j=1}^{\infty} (-1)^j \left(\frac{r^{j-1}}{j^{m-1}} \right) \right], \end{aligned} \quad (\text{D.9})$$

where $\frac{r^{j-1}}{j^{m-1}} > \frac{r^j}{(j+1)^{m-1}}$ and $\lim_{j \rightarrow \infty} \left[\frac{r^{j-1}}{j^{m-1}} \right] = 0$. Then, by the Leibniz criterion, the alternating series of $\frac{d}{dr} [\text{Li}_m[-r]]$ converge to a finite limit L . Using the bounds in Eq. (D.3) for $n = 1$ it holds that

$$S_2 \leq L \leq S_3. \quad (\text{D.10})$$

The partial sum for the even number of terms is

$$\begin{aligned} S_2 &= -\frac{r^0}{1^{m-1}} + \frac{r^1}{2^{m-1}} \\ &= -1 + \frac{r}{2^{m-1}} < 0 \quad \forall r \in [0, 1] \end{aligned} \quad (\text{D.11})$$

because S_2 increases linearly in r but is always negative since we have at the extremes $S_2 = -1$ when $r = 0$ and $S_2 = -1 + \frac{1}{2^{m-1}} < 0$ when $r = 1$ for $m \in \{2, 3, 4, \dots\}$. Similarly, we have for the partial sum with an odd number of terms

$$\begin{aligned} S_3 &= -1 + \frac{r}{2^{m-1}} - \frac{r^2}{3^{m-1}} \\ &= S_2 - \frac{r^2}{3^{m-1}} < 0 \end{aligned} \quad (\text{D.12})$$

because $S_2 < 0$ and $-\frac{r^2}{3^{m-1}} < 0 \quad \forall r \in [0, 1], m \in \{2, 3, 4, \dots\}$. Consequently, we have that

$$\begin{aligned} \frac{d}{dr} [f\text{Li}_m[-r]] &= f \frac{d}{dr} [\text{Li}_m[-r]] \\ &= fL < 0 \quad \forall r \in [0, 1], \end{aligned} \quad (\text{D.13})$$

with $m \in \{2, 3, 4, \dots\}$. By inequalities (D.8) and (D.13) it holds that

$$\begin{aligned} \frac{d}{dr} [f\text{Li}_m[-r]] &< 0 \quad \forall r \in [0, 1], \\ m &\in \{1, 2, 3, \dots\}, \end{aligned} \quad (\text{D.14})$$

and hence the function $f\text{Li}_m[-r]$ is strictly decreasing for $r \in [0, 1]$ and $m \in \{1, 2, 3, \dots\}$.

Shifted-geometric exponential density

Next, we prove the decreasing property for the shifted-geometric function in the shifted-geometric exponential density in Eq. (39). The derivative of the function is

$$\begin{aligned} \frac{d}{dr} \left[f \left(\frac{1}{1 + \tau r} - 1 \right) \right] &= f \frac{d}{dr} \left[\left(\frac{1}{1 + \tau r} - 1 \right) \right] \\ &= f \frac{d}{dr} \left[(1 + \tau r)^{-1} \right] \\ &= -\frac{f\tau}{(1 + \tau r)^2} < 0 \quad \forall r \in [0, 1] \end{aligned} \quad (\text{D.15})$$

because $f > 0$, $\tau > 0$ and $(1 + \tau r)^2 > 0$. It follows that the function $f \left(\frac{1}{1 + \tau r} - 1 \right)$ is strictly decreasing for $r \in [0, 1]$ and $0 < \tau < 1$.

Appendix D.3. Integrals for the shifted-geometric exponential distribution

We now verify the definite integral result from Eq. (40). Since $F(u|f, \tau)$ denotes the distribution function evaluated at u we have that

$$F(1|f, \tau) = \frac{1}{Z} \int_0^1 \exp \left[f \left(\frac{1}{1 + \tau r} - 1 \right) \right] dr = 1. \quad (\text{D.16})$$

From Eq. (D.16), we obtain the normalization constant

$$\begin{aligned} Z &= \int_0^1 \exp \left[f \left(\frac{1}{1 + \tau r} - 1 \right) \right] dr \\ &= \left(\frac{1 + \tau r}{\tau} \exp \left[f \left(\frac{1}{1 + \tau r} - 1 \right) \right] - \frac{f e^{-f}}{\tau} \text{Ei} \left(\frac{f}{1 + \tau r} \right) \right) \Big|_0^1. \end{aligned} \quad (\text{D.17})$$

The last right hand side of Eq. (D.17) contains the indefinite integral of $\exp \left[f \left(\frac{1}{1 + \tau r} - 1 \right) \right] dr$ to be evaluated from 0 to 1. We now obtain the derivative of such an indefinite integral. For this we make use of the series representation of the special exponential integral function $\text{Ei}(x)$ when its argument x is real, defined in Eq. (41). The derivative is then

$$\begin{aligned} & \frac{d}{dr} \left[\frac{1 + \tau r}{\tau} \exp \left[f \left(\frac{1}{1 + \tau r} - 1 \right) \right] - \frac{f e^{-f}}{\tau} \text{Ei} \left(\frac{f}{1 + \tau r} \right) \right] \\ &= \frac{d}{dr} \left[\frac{1 + \tau r}{\tau} \exp \left[f \left(\frac{1}{1 + \tau r} - 1 \right) \right] - \frac{f e^{-f}}{\tau} \left(\gamma + \log \left(\frac{f}{1 + \tau r} \right) + \sum_{k=1}^{\infty} \frac{\left(\frac{f}{1 + \tau r} \right)^k}{k k!} \right) \right] \\ &= \left(-\frac{f}{(1 + \tau r)^2} + 1 - \tau r \frac{f}{(1 + \tau r)^2} \right) \exp \left[f \left(\frac{1}{1 + \tau r} - 1 \right) \right] + \\ & \quad \left(-\frac{f e^{-f}}{\tau} \left[-\frac{\tau f^0 (1 + \tau r)^{-1}}{0!} - \frac{\tau f^1 (1 + \tau r)^{-2}}{1!} - \frac{\tau f^2 (1 + \tau r)^{-3}}{2!} - \dots \right] \right) \\ &= \left(1 - \left(\frac{f}{(1 + \tau r)^2} (1 + \tau r) \right) \right) \exp \left[f \left(\frac{1}{1 + \tau r} - 1 \right) \right] + \\ & \quad \left(\frac{f}{1 + \tau r} \right) e^{-f} \sum_{k=1}^{\infty} \frac{\left(\frac{f}{1 + \tau r} \right)^{k-1}}{(k-1)!} \\ &= \left(1 - \frac{f}{1 + \tau r} \right) \exp \left[f \left(\frac{1}{1 + \tau r} - 1 \right) \right] + \left(\frac{f}{1 + \tau r} \right) e^{-f} \sum_{k=0}^{\infty} \frac{\left(\frac{f}{1 + \tau r} \right)^k}{(k)!} \\ &= \left(1 - \frac{f}{1 + \tau r} \right) \exp \left[f \left(\frac{1}{1 + \tau r} - 1 \right) \right] + \left(\frac{f}{1 + \tau r} \right) e^{-f} \exp \left[\frac{f}{1 + \tau r} \right] \\ &= \exp \left[f \left(\frac{1}{1 + \tau r} - 1 \right) \right]. \end{aligned} \quad (\text{D.18})$$

Hence by Eq. (D.18) we have that

$$\begin{aligned} & \int_0^u \exp \left[f \left(\frac{1}{1 + \tau r} - 1 \right) \right] dr \\ &= \left(\frac{1 + \tau r}{\tau} \exp \left[f \left(\frac{1}{1 + \tau r} - 1 \right) \right] - \frac{f e^{-f}}{\tau} \text{Ei} \left(\frac{f}{1 + \tau r} \right) \right) \Big|_0^u, \end{aligned} \quad (\text{D.19})$$

which is the integral used to obtain Z in Eq. (D.17) and which also defines the distribution function in Eq. (40).

Integrals to compute the mean and the variance

The integral for the mean value in Eq. (42) is

$$\mu_R = \frac{1}{2Z} \left[\frac{\tau r - 1}{\tau} \int \exp \left[f \left(\frac{1}{1 + \tau r} - 1 \right) \right] dr + \frac{f e^{-f}}{\tau} \int \text{Ei} \left(\frac{f}{1 + \tau r} \right) dr \right] \Big|_0^1, \quad (\text{D.20})$$

where the normalization constant Z is given in Eq. (D.17) and the improper integral over the exponential shifted-geometric function is given in Eq. (D.19) (without evaluating over the limits). The improper integral over the special exponential integral function is

$$\begin{aligned} \int \text{Ei} \left(\frac{f}{1 + \tau r} \right) dr &= \gamma r + \frac{1 + \tau r}{\tau} \log \left(\frac{f}{1 + \tau r} \right) + r \\ &+ \frac{f}{\tau} \log(1 + \tau r) - \sum_{k=2}^{\infty} \frac{f^k (1 + \tau r)^{-(k-1)}}{k k! \tau (k-1)} + C_1, \end{aligned} \quad (\text{D.21})$$

with C_1 an integration constant.

The integral for the variance in Eq. (43) is

$$\begin{aligned} \sigma_R^2 &= \frac{1}{3Z} \left[\frac{1 + \tau r^2}{\tau} \int \exp \left[f \left(\frac{1}{1 + \tau r} - 1 \right) \right] dr \right. \\ &+ 2 \frac{f e^{-f}}{\tau} \int \text{Ei} \left(\frac{f}{1 + \tau r} \right) r dr \\ &- \frac{1}{\tau} \int \exp \left[f \left(\frac{1}{1 + \tau r} - 1 \right) \right] dr \\ &\left. - \frac{2}{\tau} \int \exp \left[f \left(\frac{1}{1 + \tau r} - 1 \right) \right] r dr \right] \Big|_0^1 - \mu_R^2, \end{aligned} \quad (\text{D.22})$$

where the normalization constant Z is given in Eq. (D.17), the improper integrals over the exponential shifted-geometric function are given by Eq. (D.19) (without evaluating over the limits). Also, the improper integral over the first moment for the shifted-geometric distribution is given in Eq. (D.20) (without evaluating the limits). Further, the improper integral of r multiplied by the special exponential integral function is

$$\int \text{Ei} \left(\frac{f}{1 + \tau r} \right) r dr = r \int \text{Ei} \left(\frac{f}{1 + \tau r} \right) dr - \int \int \text{Ei} \left(\frac{f}{1 + \tau r} \right) dr' dr. \quad (\text{D.23})$$

In turn, the iterated integral in Eq. (D.23) is

$$\begin{aligned} \int \int \text{Ei} \left(\frac{f}{1 + \tau r} \right) dr' dr &= \frac{1}{\tau} \int \log \left(\frac{f}{1 + \tau r} \right) dr + \int r \log \left(\frac{f}{1 + \tau r} \right) dr \\ &\quad + \frac{f}{\tau} \int \log(1 + \tau r) dr \\ &\quad + \frac{1}{2} (r^2 + \gamma r^2) - \frac{f^2}{4\tau^2} \log(1 + \tau r) \\ &\quad + \sum_{k=3}^{\infty} \frac{f^k (1 + \tau r)^{-(k-2)}}{\tau^2 k (k-1) (k-2) k!}, \end{aligned} \quad (\text{D.24})$$

with the integrals over the logarithmic functions

$$\frac{1}{\tau} \int \log \left(\frac{f}{1 + \tau r} \right) dr = \frac{1}{\tau} \left[\frac{1 + \tau r}{\tau} \log \left(\frac{f}{1 + \tau r} \right) + r \right] + C_2, \quad (\text{D.25})$$

$$\int \log \left(\frac{f}{1 + \tau r} \right) r dr = \frac{1}{2} \left[\frac{\tau r - 1}{\tau} \int \log \left(\frac{f}{1 + \tau r} \right) dr - \frac{1}{2} r^2 \right] + C_3, \quad (\text{D.26})$$

and

$$\frac{f}{\tau} \int \log(1 + \tau r) dr = \frac{f}{\tau} \left[r \log(1 + \tau r) - r + \frac{1}{\tau} \log(1 + \tau r) \right] + C_4, \quad (\text{D.27})$$

with C_2, C_3 and C_4 integration constants.

Appendix D.4. Entropy

Entropy for the polylogarithmic exponential distribution

For the polylogarithmic exponential distribution ($m = 1$), the entropy is

$$\mathbb{E}_R [-\log(p(r|f, m = 1))]$$

$$\begin{aligned}
&= - \int_0^1 \frac{1}{Z} \exp[-f \log(1+r)] \log\left(\frac{1}{Z} \exp[-f \log(1+r)]\right) dr \\
&= \int_0^1 \frac{1}{Z} \frac{1}{(1+r)^f} \log\left((1+r)^f\right) dr + \log(Z) \\
&= \frac{1}{Z} \left[\left(-\frac{f \log(1+r)}{(f-1)(1+r)^{f-1}} - \frac{f}{(f-1)^2(1+r)^{f-1}} \right) \Big|_0^1 \right] + \log(Z) \\
&= \frac{f}{1-2^{-f+1}} \left[\frac{1}{(f-1)} - \frac{\log 2}{2^{f-1}} - \frac{1}{(f-1)2^{f-1}} \right] \\
&\quad + \log\left(\frac{1-2^{-f+1}}{f-1}\right) \quad f \neq 1, \tag{D.28}
\end{aligned}$$

and where

$$\begin{aligned}
&\mathbb{E}_R[-\log(p(r|f=1, m=1))] \\
&= \frac{1}{Z} \left[\frac{1}{2} (\log(1+r))^2 \Big|_0^1 \right] + \log(Z) \\
&= \frac{1}{2} \log 2 + \log(\log 2) \quad f = 1. \tag{D.29}
\end{aligned}$$

Entropy for the shifted-geometric exponential distribution

The entropy of the shifted-geometric exponential distribution is

$$\begin{aligned}
&\mathbb{E}_R[-\log(p(r|f, \tau))] \\
&= - \int_0^1 \frac{1}{Z} \exp\left[f \left(\frac{1}{1+\tau r} - 1\right)\right] \log\left(\frac{1}{Z} \exp\left[f \left(\frac{1}{1+\tau r} - 1\right)\right]\right) dr \\
&= \log(Z) - \frac{f}{Z} \int_0^1 \left(\exp\left[f \left(\frac{1}{1+\tau r} - 1\right)\right] \frac{1}{1+\tau r} \right) dr + f \\
&= \log(Z) - \frac{f e^{-f} \left(\text{Ei}(f) - \text{Ei}\left(\frac{f}{1+\tau}\right) \right)}{(1+\tau) \exp\left[f \left(\frac{1}{1+\tau} - 1\right)\right] + f e^{-f} \left(\text{Ei}(f) - \text{Ei}\left(\frac{f}{1+\tau}\right) \right) - 1} + f, \tag{D.30}
\end{aligned}$$

To obtain the last equality, we computed the integral in the second term as follows

$$\begin{aligned}
&\frac{f}{Z} \int_0^1 \exp\left[f \left(\frac{1}{1+\tau r} - 1\right)\right] \frac{1}{1+\tau r} dr \\
&= \frac{1}{Z} \left(\frac{1+\tau r}{\tau} \exp\left[f \left(\frac{1}{1+\tau r} - 1\right)\right] - \frac{f e^{-f}}{\tau} \text{Ei}\left(\frac{f}{1+\tau r}\right) \right)
\end{aligned}$$

$$\begin{aligned}
& -\frac{1+\tau r}{\tau} \exp \left[f \left(\frac{1}{1+\tau r} - 1 \right) \right] \Big|_0^1 \\
= & \frac{1}{Z} \left[\frac{1+\tau}{\tau} \exp \left[f \left(\frac{1}{1+\tau} - 1 \right) \right] - \frac{f e^{-f}}{\tau} \text{Ei} \left(\frac{f}{1+\tau} \right) \right. \\
& \quad \left. - \frac{1+\tau}{\tau} \exp \left[f \left(\frac{1}{1+\tau} - 1 \right) \right] \right. \\
& \quad \left. - \frac{1}{\tau} + \frac{f e^{-f}}{\tau} \text{Ei} (f) + \frac{1}{\tau} \right] \\
= & \frac{f e^{-f} \left(\text{Ei} (f) - \text{Ei} \left(\frac{f}{1+\tau} \right) \right)}{(1+\tau) \exp \left[f \left(\frac{1}{1+\tau} - 1 \right) \right] + f e^{-f} \left(\text{Ei} (f) - \text{Ei} \left(\frac{f}{1+\tau} \right) \right) - 1}. \tag{D.31}
\end{aligned}$$

Appendix D.5. Heat capacity

Heat capacity for the polylogarithmic exponential distribution

The normalization constant and the derivatives of the heat capacity (Eq. (47)) corresponding to the polylogarithmic exponential distribution ($m = 1$) with $f \neq 1$ are as follows

$$Z = \frac{1 - 2^{-f+1}}{f - 1}, \tag{D.32}$$

$$\frac{dZ}{df} = \frac{2^{-f+1} \log 2}{f - 1} - \frac{(1 - 2^{-f+1})}{(f - 1)^2}, \tag{D.33}$$

and

$$\frac{d^2 Z}{(df)^2} = -\frac{2^{-f+1} (\log 2)^2}{(f - 1)} - \frac{2^{-f+2} \log 2}{(f - 1)^2} + \frac{2(1 - 2^{-f+1})}{(f - 1)^3}. \tag{D.34}$$

We now show that the limit is 1 for the heat capacity of the polylogarithmic exponential distribution ($m = 1$) as $f \rightarrow \infty$.

$$\lim_{f \rightarrow \infty} C(f) = \lim_{f \rightarrow \infty} \left[\frac{f^2 \frac{d^2}{(df)^2} Z - f^2 \left(\frac{dZ}{df} \right)^2}{Z^2} \right], \tag{D.35}$$

where

$$f^2 \frac{d^2 Z}{(df)^2} Z = \frac{2f^2 Z^2}{(f - 1)^2} - f^2 Z \left(\frac{2^{-f+1} \log^2 2}{f - 1} + \frac{2^{-f+1} \log 4}{(f - 1)^2} \right), \tag{D.36}$$

and

$$f^2 \left(\frac{dZ}{df} \right)^2 = f^2 \left(\frac{2^{-2f+2} \log^2 2}{(f-1)^2} - \frac{2^{-f+1} \log 4}{(f-1)^2} Z + \frac{Z^2}{(f-1)^2} \right). \quad (\text{D.37})$$

Then, continuing with Eq. (D.35) we obtain the following limit

$$\begin{aligned} \lim_{f \rightarrow \infty} C(f) &= \lim_{f \rightarrow \infty} \left[\frac{\frac{f^2}{(f-1)^2} Z^2 - \frac{f^2 2^{-f+2} \log^2 2}{(f-1)} Z - \frac{f^2 2^{-2f+2} \log^2 2}{(f-1)^2}}{Z^2} \right] \\ &= \frac{\lim_{f \rightarrow \infty} \frac{f^2 Z^2}{(f-1)^2} - \lim_{f \rightarrow \infty} \left(\frac{f^2 2^{-f+1} \log^2 2}{f-1} Z + \frac{f^2 2^{-2f+2} \log^2 2}{(f-1)^2} \right)}{\lim_{f \rightarrow \infty} Z^2} \\ &= \lim_{f \rightarrow \infty} \frac{f^2 Z^2}{(f-1)^2 Z^2} - 0 = 1. \end{aligned} \quad (\text{D.38})$$

Heat capacity for the shifted-geometric exponential distribution

Similarly to the polylogarithmic case, for the heat capacity of the shifted-geometric exponential distribution we obtain

$$Z = \frac{1+\tau}{\tau} \exp \left[f \left(\frac{1}{1+\tau} - 1 \right) \right] + \frac{f e^{-f}}{\tau} \left(\text{Ei}(f) - \text{Ei} \left(\frac{f}{1+\tau} \right) \right) - \frac{1}{\tau}, \quad (\text{D.39})$$

$$\frac{dZ}{df} = -\frac{1+\tau}{\tau} \exp \left[f \left(\frac{1}{1+\tau} - 1 \right) \right] + \frac{1}{\tau} + \frac{1-f}{\tau} e^{-f} \left(\text{Ei}(f) - \text{Ei} \left(\frac{f}{1+\tau} \right) \right) \quad (\text{D.40})$$

and

$$\begin{aligned} \frac{d^2 Z}{(df)^2} &= \frac{1+\tau-f^{-1}}{\tau} \exp \left[f \left(\frac{1}{1+\tau} - 1 \right) \right] + \frac{1-f}{f\tau} \\ &\quad + \frac{e^{-f}}{\tau} (f-2) \left(\text{Ei}(f) - \text{Ei} \left(\frac{f}{1+\tau} \right) \right). \end{aligned} \quad (\text{D.41})$$

Appendix D.6. Sparsity

For the case of large f we consider the shifted-geometric case and the increasing sequence $s_k(r) = 1 - \exp \left[-f_k \left(1 - \frac{1}{1+\tau r} \right) \right]$ with $f_k > 0$. Then, by the Beppo Levi's lemma:

$$\begin{aligned} \lim_{k \rightarrow \infty} \int_0^1 s_k(r) dr &= \int_0^1 \lim_{k \rightarrow \infty} s_k(r) dr \\ &= \int_0^1 \lim_{k \rightarrow \infty} \left(1 - \exp \left[-f_k \left(1 - \frac{1}{1+\tau r} \right) \right] \right) dr \end{aligned}$$

$$\begin{aligned}
&= \int_0^1 1dr - \int_0^1 \lim_{k \rightarrow \infty} \exp \left[-f_k \left(1 - \frac{1}{1 + \tau r} \right) \right] dr \\
&= r \Big|_0^1 - \int_0^1 \lim_{f \rightarrow \infty} \exp \left[-f \left(1 - \frac{1}{1 + \tau r} \right) \right] dr \\
&= 1 - \int_0^1 0dr \\
&= 1.
\end{aligned} \tag{D.42}$$

From the previous, we can see that

$$\begin{aligned}
1 - \int_0^1 \lim_{k \rightarrow \infty} \exp \left[-f_k \left(1 - \frac{1}{1 + \tau r} \right) \right] dr &= \lim_{k \rightarrow \infty} \int_0^1 s_k(r) dr \\
&= \lim_{k \rightarrow \infty} \left(\int_0^1 1dr - \int_0^1 \exp \left[-f_k \left(1 - \frac{1}{1 + \tau r} \right) \right] dr \right) \\
&= 1 - \lim_{k \rightarrow \infty} \int_0^1 \exp \left[-f_k \left(1 - \frac{1}{1 + \tau r} \right) \right] dr,
\end{aligned} \tag{D.43}$$

which yields

$$\begin{aligned}
\lim_{k \rightarrow \infty} \int_0^1 \exp \left[-f_k \left(1 - \frac{1}{1 + \tau r} \right) \right] dr &= \lim_{f \rightarrow \infty} \int_0^1 \exp \left[-f \left(1 - \frac{1}{1 + \tau r} \right) \right] dr \\
&= \int_0^1 \lim_{k \rightarrow \infty} \exp \left[-f_k \left(1 - \frac{1}{1 + \tau r} \right) \right] dr \\
&= \int_0^1 \lim_{f \rightarrow \infty} \exp \left[-f \left(1 - \frac{1}{1 + \tau r} \right) \right] dr \\
&= 0,
\end{aligned} \tag{D.44}$$

where the dependence on k is replaced by simply considering the limit of f directly, which is equivalent.

Then, considering Eq. (D.44), the limit for the actual PDF becomes

$$\begin{aligned}
\lim_{f \rightarrow \infty} p(r|f, \tau) &= \frac{\lim_{f \rightarrow \infty} \exp \left[-f \left(1 - \frac{1}{1 + \tau r} \right) \right]}{\lim_{f \rightarrow \infty} \int_0^1 \exp \left[-f \left(1 - \frac{1}{1 + \tau r} \right) \right] dr} \\
&= \frac{\lim_{f \rightarrow \infty} \exp \left[-f \left(1 - \frac{1}{1 + \tau r} \right) \right]}{\int_0^1 \lim_{f \rightarrow \infty} \exp \left[-f \left(1 - \frac{1}{1 + \tau r} \right) \right] dr} \\
&= \frac{1}{0} \mathbb{1}_{[r=0]} \\
&= \delta(r).
\end{aligned} \tag{D.45}$$

Similarly $\lim_{f \rightarrow \infty} p(r|f, m) = \delta(r)$. For the latter, we omit the proof, but it follows similarly using now the increasing sequence $s_k(r) = 1 - \exp[f_k \text{Li}_m[-r]]$.